MOL.20060825.0208

DT# 47406 QA:NA Cb 8/3/06

Analyzing Unsaturated Flow Patterns in Fractured Rock Using an Integrated Modeling Approach

Yu-Shu Wu, Guoping Lu, Keni Zhang, Lehua Pan, and Gudmundur S. Bodvarsson

Lawrence Berkeley National Laboratory
Berkeley CA 94720 USA

Abstract

Characterizing percolation patterns in unsaturated fractured rock has posed a greater challenge to modeling investigations than comparable saturated zone studies, because of the heterogeneous nature of unsaturated media and the great number of variables impacting unsaturated flow. This paper presents an integrated modeling methodology for quantitatively characterizing percolation patterns in the unsaturated zone of Yucca Mountain, Nevada, a proposed underground repository site for storing high-level radioactive waste. The modeling approach integrates a wide variety of moisture, pneumatic, thermal, and isotopic geochemical field data into a comprehensive three-dimensional numerical model for modeling analyses. It takes into account the coupled processes of fluid and heat flow and chemical isotopic transport in Yucca Mountain's highly heterogeneous, unsaturated fractured tuffs. Modeling results are examined against different types of field-measured data and then used to evaluate different hydrogeological conceptualizations and their results of flow patterns in the unsaturated zone. In particular, this model provides a much clearer understanding of percolation patterns and flow behavior through the unsaturated zone, both crucial issues in assessing repository performance. The integrated approach for quantifying Yucca Mountain's flow system is demonstrated to provide a practical modeling tool for characterizing flow and transport processes in complex subsurface systems.

1. Introduction

Since the 1980s, the unsaturated zone (UZ) of the highly heterogeneous, fractured tuff at Yucca Mountain, Nevada, the U.S. has been investigated as a possible repository site for storing high-level radioactive waste. Characterization of flow and transport processes in the fractured rock of the Yucca Mountain UZ has received significant attention and generated substantial interest in scientific communities over the last two decades. During this period of extensive studies, many types of data have been collected from the Yucca Mountain UZ, and these data have helped in developing a conceptual understanding of various physical processes within the UZ system.

While quantitative evaluation of fluid flow, chemical transport, and heat transfer has proven to be essential, the complexity of geological conditions and physical processes within the Yucca Mountain UZ has posed a tremendous challenge for site characterization efforts. The need for quantitative investigations of flow and transport at the Yucca Mountain site has motivated an ongoing effort to develop and apply large, mountain-scale flow and transport models [*e.g., Wu et al.*, 1999a and 2002a]. Numerical models have played a crucial role in our understanding of UZ fluid movement in assessing the effects of hydrogeological, geochemical, and thermal conditions on various aspects of the overall waste disposal system. Whereas laboratory studies and field experiments, however necessary, are limited in space and time, numerical modeling provides a powerful means by which to study physical processes on the temporal and spatial scales relevant to the understanding of the nuclear waste disposal systems in a geological formation.

Site characterization studies of the unsaturated tuff at the Nevada Test Site and at Yucca Mountain began in the late 1970s and early 1980s. Those early hydrological, geological, and geophysical investigations of Yucca Mountain and its surrounding region were conducted to assess the feasibility of the site as a geological repository for storing high-level radioactive waste, and to provide conceptual understanding of UZ flow processes [*Montazer and Wilson,* 1984]. Soon after, as part of the continuing site characterization, theoretical studies were deemed necessary to quantitatively model unsaturated groundwater flow. The first numerical modeling effort was made in the middle 1980s to simulate the natural state of the UZ underlying Yucca Mountain, using a two-dimensional site-scale model [*Rulon et al.,* 1986]. This work was followed by a number of other modeling efforts, focused on more basic-level processes. *Pollock* [1986] developed a mathematical model for analyzing one-dimensional, vertical transport of energy, water, and air in unsaturated alluvium. *Tsang* and *Pruess* [1987] studied thermally induced convection phenomena near a high-level nuclear waste repository in partially saturated tuff, using a two-dimensional model. *Weeks* [1987] reported a study of gas flow in the Yucca Mountain UZ to explain air circulation as observed from boreholes.

In the early 1990s, more progress was made in UZ model development. *Wittwer et al.* [1992, 1995] developed a three-dimensional (3-D) site-scale model that incorporated several geological and hydrological complexities, such as geological layering, degree of welding, fault offsets, and different matrix and fracture properties. The 3-D model handled fracture-matrix flow using an effective continuum method (ECM) and was applied to evaluate assumptions concerning faults and infiltration patterns.

Using the ECM concept, *Ahlers et al.* [1995a, 1995b] continued development of the UZ site-scale model with increased numerical and spatial resolution. Their studies considered more processes, such as gas and heat flow analyses, and introduced an inverse modeling approach for estimating model-input properties. However, more comprehensive UZ models were not developed until several years later, when the UZ models were developed for Total System Performance Assessment–Viability Assessment (TSPA-VA) [*e.g., Wu et al.,* 1999a and 1999b; *Bandurraga and Bodvarsson,* 1999; *Ahlers et al.,* 1999]. Instead of the ECM, the TSPA-VA model used a more rigorous dual-permeability numerical approach for handling fracture-matrix interaction and incorporated additional physical processes, such as perched-water occurrence.

The latest UZ models include those primarily developed for the TSPA site recommendation (SR) calculations [*e.g., Wu et al.,* 2002a; *Moridis et al.,* 2003; *Robinson et al.,* 2003]. These TSPA-SR models have been enhanced from the TSPA-VA model. More importantly, the newer models have taken into account the coupled processes of flow and transport in highly heterogeneous, unsaturated fractured rock, and were applied to analyzing the effect of current and future climates on radionuclide transport through the UZ system. The site-scale UZ flow and transport models developed during the site characterization of Yucca Mountain have built upon past research as well as the above-referenced work and many other studies [*e.g., McLaren et al.,* 2000; *Robinson et al.,* 1996 and 1997; *Viswanathan et al.,* 1998; *Sonnenthal and Bodvarsson,* 1999; *Liu et al.,* 2003]. In general, model development, benefiting significantly from extensive field and laboratory studies of the site, has followed an iterative or trial-and-error approach [*Wu et al.,* 2002a].

Despite the significant progress made in the site characterization of the Yucca Mountain UZ over the last two decades, there is still a general lack of comprehensive analyses or integrated studies related to the site. In particular, little effort has been made to make use of all available data from different types and sources in one study. Previous investigations, for example, were focused primarily on separate studies of moisture data [e.g., *Wu et al.,* 1999a; 2002a], temperature data [e.g., *Bovardsson et al.,* 2003], pneumatic data [e.g., *Ahlers et al.,* 1999], or chloride data [e.g., Liu et al., 2003]. How to quantitatively analyze percolation flux in the deep unsaturated zone, such as within the complicated unsaturated fracture-matrix system of Yucca Mountain, remains a great challenge to investigators [e.g., *Flint et al.,* 2002]. (Percolation flux is defined as total vertical-liquid mass flux through both fractures and matrix, and is converted to millimeters per year (mm/yr) per unit area using a constant water density). The main difficulties are (1) that unsaturated percolation flux is too low to measure directly and (2) flow paths are too complicated to identify in field studies. To the best of our knowledge, no commonly accepted approaches exist for directly measuring or quantifying unsaturated percolation fluxes on the spatial and temporal scales of interest to the Yucca Mountain Project. In an attempt to overcome these difficulties, we propose a comprehensive, integrated modeling approach, which incorporates everything measured at the site, including hydrological, pneumatic, geochemical, and thermal data, into an integrated numerical modeling analysis, for the purpose of analyzing percolation patterns and behavior.

This paper presents an integrated modeling methodology for characterizing percolation flux in unsaturated fracture rock. In particular, a comprehensive modeling effort is made to quantify moisture movement at the Yucca Mountain site. The multiple processes under study include moisture flow, natural geochemical or tracer transport, and gas and heat flow. The modeling results of the multiple processes, using the integrated modeling approach, provide a better understanding of percolation patterns and flow behavior within the Yucca Mountain UZ under different climates and hydrogeological conceptual models of UZ flow. First, this present effort discusses integration of different field-observed data, such as water potential, liquid saturation, perched water, gas pressure, chloride, and temperature logs, into one single 3-D UZ flow and transport model. The combined model calibration will provide a consistent cross-check or verification of modeled percolation fluxes, as well as better insight into UZ flow patterns. Second, using the dual-permeability modeling approach, a more rigorous method for modeling fracture-matrix interaction [Wu et al. 1999a], this integrated modeling effort provides consistent model predictions for different but interrelated hydrological, pneumatic, geochemical, and geothermal processes in the UZ. Third, and most importantly, such an integrated approach will improve the capability and credibility of numerical models in characterizing flow and transport processes in unsaturated fractured formation in general.

This work presents our continual efforts in developing and applying the UZ flow and transport models in characterizing the UZ system of Yucca Mountain. Specifically, this modeling study consists of (1) a brief UZ model description; (2) model calibration using pneumatic data, while calibrations using moisture and geochemical data are reported in *BSC* [2004] and *Wu et al.* [2004]; (3) simulated percolation pattern analysis; and (4) assessing percolation patterns and flow behavior using thermal and geochemical data.

2. Hydrogeological Setting, Physical Process, and Conceptualization

The domain of the UZ model encompasses approximately 40 km^2 of the Yucca Mountain area, as shown in Figure 1. The UZ is between 500 and 700 m thick and overlies a relatively flat water table. The repository would be located in the highly fractured Topopah Spring welded tuff unit, more than 200 m above the water table. Geologically, Yucca Mountain is a structurally complex system of Tertiary volcanic rock. Subsurface hydrological processes in the UZ occur in a heterogeneous environment of layered, anisotropic, and fractured volcanic rocks [*Scott and Bonk*, 1984]. These volcanic formations consist of alternating layers of welded and nonwelded ash flow and air-fall tuffs. The primary geological formations, beginning from the land surface and progressing downward, are the Tiva Canyon, Yucca Mountain, Pah Canyon, and the Topopah Spring tuffs of the Paintbrush Group. Underlying these are the Calico Hills Formation and the Prow Pass, Bullfrog, and Tram tuffs of the Crater Flat Group [*Buesch et al.*, 1995].

For hydrological investigations, the UZ geologic formations have been categorized into hydrogeologic units based primarily on their degree of welding [*Montazer and Wilson*, 1984]. These units are classified as the Tiva Canyon welded (TCw) hydrogeologic unit; the Paintbrush Tuff nonwelded unit (PTn), consisting primarily of the Yucca Mountain and Pah Canyon bedded tuffs; the Topopah Spring welded (TSw) unit; the Calico Hills nonwelded (CHn) unit; and the Crater Flat undifferentiated (CFu) unit. The hydrogeological units vary significantly in thickness and sloping over the model domain (Figure 2).

Conceptual Model of UZ Flow

Over the past two decades, extensive scientific investigations have been conducted for the site characterization of Yucca Mountain, including collecting data from surface mapping, sampling from many deep and shallow boreholes, constructing underground tunnels, and conducting field testing [e.g., *Rousseau,* 1998]. Figure 2 presents a typical geological profile along a vertical east-west transect of borehole UZ-14 (Figure 1), illustrating a conceptual model currently used to analyze UZ flow patterns, as well as explaining the possible effects of faults and perched water on the UZ system. As illustrated in Figure 2, the ground surface of the UZ is subject to spatially and temporally varying infiltration pulses from precipitation, which provide the water source for deep percolation into the UZ. Surface infiltration pulses are expected to move rapidly through the top, highly fractured TCw unit. Once it enters the PTn, percolating water may be subject to very different processes, because the PTn unit has very different hydrogeologic properties from the TCw and TSw units, which display the low porosity and intensive fracturing typical of densely welded tuffs. With its high porosity and low fracture intensity, the PTn matrix has a large capacity for storing groundwater. As a result, moisture imbibing into the relatively dry PTn matrix from rapid fracture flow of the TCw may result in a more uniform distribution of flux at the base of the PTn. In fact, the PTn's capability to attenuate episodic percolation fluxes has been observed in field tests of water release into the PTn matrix [*Salve et al.*, 2003].

In addition, the possibility for capillary barriers exists at both upper and lower PTn contacts, as well as within the PTn layers [*Montazer and Wilson*, 1984; *Wu et al.* 2002b], because large contrasts in rock properties exist across the interfaces of units and inner PTn layers. However, the extent of lateral flow diversion within the PTn remains a topic of debate. For example, a recent study using a concept with transitional changes in rock properties argues that lateral diversion may be small [*Flint et al.,* 2003].

Perched Water

Perched water has been encountered in a number of boreholes at Yucca Mountain, including UZ-14, SD-7, SD-9, SD-12, NRG-7a, G-2, and WT-24 (Figure 1). These perched-water locations are found to be associated with low-permeability zeolites in the CHn or the densely welded basal vitrophyre of the TSw unit, below the repository horizon. Perched water is another important mechanism impacting flow paths in the UZ units below the repository horizon.

Perched water may occur where percolation flux exceeds the capacity of the geological media to transmit vertical flux in the UZ [*Rousseau et al.*, 1998]. Several conceptual models for perched water have been investigated for explaining the genesis of perched water at Yucca Mountain [*e.g., Wu et al.*, 1999b and 2002a]. The permeability-barrier conceptual model, for one example, has been used in UZ flow modeling studies since 1996 [*Wu et al.,* 1999b and 2002a]. In this conceptual model, both vertical and lateral water movement in the vicinity of the perched zones is considered to be controlled mainly by localized fracture and matrix permeability distributions. The main assumptions of the permeability-barrier conceptual model are that: (1) there are few large, vertically connected, potentially fluid-conducting fractures transecting the underlying low-permeability units; (2) both vertical and horizontal permeabilities within and below perched-water zones are small compared to permeabilities outside perching zones; and (3) sufficient percolation flux (>1 mm/yr) exists locally.

Faults

In addition to possible capillary and permeability barriers, major faults in the UZ are also expected to play an important role in controlling percolation flux. Permeability within faults is much higher than that in the surrounding tuff [*Montazer and Wilson,* 1984]. Pneumatic permeability measurements taken along portions of faults have revealed low air-entry pressures, indicating that large fracture apertures are present in the fault zones. High permeability fault zones with large pore space may act as vertical capillary barriers to lateral flow. Once water is diverted into a fault zone, however, its high permeability could facilitate rapid downward flow along faults through the unsaturated system [*Wang and Narasimhan,* 1987; *Wu et al.,* 2002a]. In this modeling study, major faults are treated as intensively fractured zones.

Heterogeneity

A considerable amount of field data, obtained from tens of boreholes, two underground tunnels, and hundreds of outcrop samples at the site, constrains the distribution of rock properties within different units. In general, field data indicate that the Yucca Mountain formation is more heterogeneous vertically than horizontally, such that layer-wise representations are found to provide reasonable approximations of the complex geological system. Many model calibration results using this approximation are able to match different types of observation data obtained from different locations and depths [*e.g., Bandurraga and Bodvarsson*, 1999; *Ahlers et al.*, 1999; *Wu et al.*, 2002a].

In summary, as shown in Figure 2, the key conceptualizations and assumptions made in this study for constructing the hydrogeological model to analyze UZ flow patterns are as follows:

- Ambient water flow in the UZ system is at a quasi-steady state condition, subject to spatially varying net infiltration on the ground surface.
- Hydrogeological units/layers are internally homogeneous, unless interrupted by faults or altered.
- There may exist capillary barriers in the PTn unit, causing lateral flow.
- Perched water results from permeability barrier effects.
- Major faults serve as fast downward flow pathways for laterally diverted flow.

3. Numerical Modeling Approach and Model Description

This section describes the modeling approach in the UZ model for handling fracture-matrix interaction, the numerical scheme and codes, numerical model grids, input parameters, and boundary conditions used in this work.

3.1 Modeling Fracture-Matrix Interaction

Modeling fracture and matrix flow and interaction under multiphase, multicomponent, isothermal, or nonisothermal conditions has been a key issue for simulating fluid and heat flow in the Yucca Mountain UZ. Different modeling approaches have been tested for handling fracture-matrix interaction at Yucca Mountain [*Doughty,* 1999]. The dual-continuum, specifically the dual-permeability concept, has been used as the main modeling approach for modeling flow and transport in the Yucca Mountain UZ [*e.g., Wu et al.,* 1999a], because it is able to simulate transient matrix-fracture interaction and account for global flow through matrix blocks, which is considered important under low percolation flux.

The technique used in this work for handling multiphase flow, tracer transport, and heat transfer through fractured rock is based primarily on the dual-permeability concept. It considers global flow and transport occurring not only between fractures but also between matrix gridblocks. In this approach, one rock-volume domain is represented by two overlapping (yet interacting) fracture and matrix continua. The fracture-matrix fluid flow is evaluated using the same quasi-steady-state approximation as in the double-porosity model [*Warren and Root*, 1963], which has also been extended in this work to estimate local mass and energy exchange terms between fracture and matrix systems [*Pruess and Narasimhan*, 1985]. When applied in this work, the traditional dual-permeability concept is first modified by using an active fracture model [*Liu et al.*, 1998] to represent fingering effects of flow through fractures. Secondly, the dual-permeability model is not used for all formation units or model domains. For example, vitric units in the CHn are handled as unfractured, single-porosity matrix only, and additional global fracture-matrix connections at boundaries of vitric units and at the TCw-PTn and PTn-TSw interfaces are considered to provide physical transitions for fracture-matrix flow across these units or domain boundaries. Therefore, the modeling approach is actually a physically based, hybrid dual-permeability model with a combination of dual-continuum and single-porosity medium approximations.

3.2 Numerical Formulation and Codes

In the dual-continuum approach, fluid flow, chemical transport, and heat transfer processes in an air-water, two-phase system of fractured rock are described separately, using a doublet of governing equations, respectively, for the two fracture and matrix continua. This conceptualization results in a set of partial differential equations for mass and energy conservation in either continuum, which are in the same form as those for a single porous medium. In this work, the multiphase flow system consists of two phases: gas (air) and water, and three mass components: air, water, and tracer. Both coupled two-phase fluid and heat flow formulation and Richards' equation (1931) are used.

Model calibration and simulation of this study were carried out using the TOUGH2 and T2R3D codes [*Pruess,* 1991; *Wu and Pruess*, 2000]. In these two TOUGH2-family codes, the integral finite-difference scheme is used for spatial discretization, and the time discretization is carried out with a backward, first-order, finite-difference scheme. The resulting discrete nonlinear algebraic equations for describing mass (or component) and/or energy conservation are written in a residual form and solved using the Newton/Raphson iteration fully implicitly with an iterative linear solver. At each time step, iteration continues until convergence is reached for a given time, when the residual at every gridblock is decreased to a preset convergence tolerance.

3.3 Numerical Model Grids

There are two 3-D numerical model grids used in this study, as shown in plan view in Figures 3a and 3b. The two 3-D UZ model grids were generated with a grid maker [*Pan et al.*, 2000], using an irregular, unstructured, 3-D control-volume spatial discretization. The first numerical grid (Figure 3a) is called the UZ flow model grid, because it is primarily designed for model calibrations and investigations of UZ flow and transport. This 3-D model grid uses a refined mesh in the vicinity of the proposed repository, located near the center of the model domain and covering the region from Solitario Canyon to Ghost Dance faults, from west to east and north to beyond Pagany Wash fault. Shown in its plan view in Figure 3b is the second 3-D model grid, covering a smaller model domain, called the thermal model grid, which is used for gas flow and ambient heat-flow modeling. Also shown in Figures 3a and 3b are the locations of a number of boreholes incorporated into model calibrations and analyses. In both model grids, faults are represented in the model by vertical or steeply inclined 30 m wide zones.

In Figures 3a and 3b, each gridblock in the x-y plane represents a vertical column defined in the 3-D grid. The 3-D flow model grid has about 2,042 mesh columns of both fracture and matrix continua along a horizontal grid layer (Figure 3a), and 50 computational grid layers in the vertical direction, resulting in 250,000 gridblocks and 1,000,000 connections in a dual-permeability grid. This 3-D flow grid is relatively large and requires extensive computational effort for simulation of coupled two-phase flow and heat transfer. This is why we designed the second, relatively smaller grid, the 3-D thermal grid (Figure 3b). As shown in the plan view of Figure 3b, the thermal model grid domain covers approximately 20 km^2 of the area. The thermal model grid of Figure 3b consists of 980 mesh columns of fracture and matrix continua, 86,440 gridblocks, and 350,000 connections in a dual-permeability grid. Vertically, the thermal grid has an average of 45 computational grid layers.

3.4 Model Input Parameters

Since Richards' and two-active-phase flow equations are used in modeling unsaturated flow of water and air through fracture and matrix, relative permeability and capillary pressure curves are needed for the two media. In addition, other intrinsic fracture and matrix properties are also needed, such as porosity, permeability, density, and fracture geometric parameters, as well as rock thermal properties. In our modeling study, the van Genuchten models of relative permeability and capillary pressure functions [*van Genuchten,* 1980] are selected to describe variably saturated flow in both fracture and matrix media. The basic input rock and fluid-flow parameters used for each model layer or hydrogeological subunit [*BSC,* 2004] include (1) fracture properties (frequency, spacing, permeability, van Genuchten α and *m* parameters, porosity, fracture-matrix interface area, and residual saturation); (2) matrix properties (porosity, permeability, the van Genuchten α and *m* parameters, and residual saturation); (3) thermal and transport properties (grain density, wet and dry thermal conductivity, grain specific heat, and diffusion and tortuosity coefficients); and (4) fault properties for each of the major hydrogeologic units.

The model input parameters for fractured and matrix rock were determined by two steps: (1) using field and laboratory measurements [*BSC,* 2003a] and 1-D model inversion results

[*BSC.,* 2003b] as an initial guess, and (2) conducting a 3-D model forward calibration, as discussed in the next section. Adopting a hybrid, dual-permeability approach, we treat all the geological units, including fault zones, as fracture-matrix systems (except for vitric zones, which are treated as single-porosity media).

3.5 Model Infiltration Boundary Conditions

The ground surface of the mountain (or the tuff-alluvium contact in the area of significant alluvial cover) is taken as the top model boundary, while the water table is treated as the bottom model boundary. For flow simulations, net infiltration is applied to fractures along the top boundary using a source term. The bottom boundary at the water table is treated as a Dirichlet-type boundary. All the lateral boundaries, as shown in Figures 1, 3a, and 3b, are treated as no-flow (laterally closed) boundaries. No-flow boundaries should have only a small effect on moisture flow and radionuclide transport within or near the repository area (which is the focus of the current study), because these lateral boundaries are either far away from the repository or separated by vertical faults.

Net infiltration of water, resulting from precipitation that penetrates the top-soil layer of the mountain, is the most important factor affecting the overall hydrological, geochemical, and thermal-hydrological behavior of the UZ. Net infiltration is the ultimate source of groundwater recharge and deep-zone percolation through the UZ, and provides a vehicle for transporting radionuclides from the repository to the water table. To cover the various possible scenarios and uncertainties of current and future climates at Yucca Mountain, we have incorporated a total of nine net infiltration maps, provided by U. S. Geological Survey (USGS) scientists [*BSC,* 2000a; *BSC,,* 2000b], into the model, These infiltration maps include present-day (modern), monsoon, and glacial transition—three climatic scenarios, each of which consists of lower-bound, mean, and upper-bound rates, as summarized in Table 1, for average rate values over the flow model domain.

As shown in Table 1, the average rate for present-day, mean infiltration with the flow model grid (Figure 3a) is 4.4 mm/yr distributed over the flow model domain, which is considered as a base-case infiltration scenario. By comparison, the thermal model grid has an average net infiltration rate of 3.6 mm/yr distributed over the smaller domain (Figure 3b) for the present-day, mean infiltration case. Note that only the present-day, mean infiltration scenario is used with the thermal grid for gas flow and ambient thermal studies. (Using lower- and upper-bound infiltration values in flow modeling is intended to cover possible higher or lower rates.) The two future Yucca Mountain climatic scenarios, the monsoon and glacial transition periods, are used to account for possible higher precipitation and infiltration conditions in the future. A plan view of the spatial distribution of the present-day mean infiltration map, as interpolated onto the flow model grid, is shown in Figure 4. The figure shows patterns of flux distributions with higher infiltration rates in the northern part of the model domain and from south to north along the mountain ridge east of the Solitario Canyon fault.

4. Model Calibration

The complexities of the heterogeneous geological formation and coupled UZ flow and transport processes at the Yucca Mountain UZ have posed serious challenges to numerical modeling investigations. For example, past modeling experiences have shown that one cannot simply input field- and laboratory-measured parameters or 1-D model inverted properties directly into 3-D models and expect reasonable simulation results. This is because of the many uncertainties and significant differences in those input parameters with respect to their spatial and temporal scales between measurements and model spatial representations. Without further calibration, those parameters observed or determined on one spatial scale are in general inappropriate for use at another spatial scale. In general, a proper model approximation of the actual physical system requires model calibration on the same model scale, from conceptual models to model parameters, as well as an accurate description of the physical processes involved.

The model calibrations for this work rely on field-measured matrix-liquid saturation, water potential, perched-water, and pneumatic data. *Liu et al.* [2003b] provide basic input parameters for fracture and matrix rock for starting modeling efforts in this paper. However, these properties were estimated through a series of 1-D model inversions in which lateral diversion, perched-water, and capillary barrier effects cannot be modeled. Use of a 3-D model allows further parameter adjustment to better match field observation data and avoid unphysical solutions. Among the various types of available data used in UZ model development, the moisture data related to matrix-liquid saturation and water potentials, measured from core samples or from *in situ* instruments, have been perhaps the most important data sources. Moisture data have been used to estimate model parameters since early model calibration efforts [*e.g., Ahlers et al.,* 1995a and 1995b] and provide a basis for current estimation of permeability and van Genuchten parameters, both for 1-D inverse modeling [*BSC.,* 2003b] and 3-D calibration [*BSC,* 2004; *Wu et al.*, 2004].

Table 2 summarizes field-measured data used in model calibration, as observed from 14 boreholes and one underground tunnel (ECRB). These data include moisture data (matrix liquid saturation, matrix water potentials, and perched-water elevations), and borehole pneumatic or gas pressure measurements.

A series of 3-D model calibrations have been carried out to estimate model-scale related parameters. The adjusted parameters include fracture-matrix properties of the top TSw layer, the entire PTn unit, and perched-water zones, as well as fracture permeabilities in the upper TSw layers. The 3-D model calibration efforts were performed in a series of forward 3-D simulations, starting with the three sets of 1-D model calibrated parameters corresponding to three rates of lower bounds, means and upper bounds of infiltration [*Liu et al.*, 2003b]. Then, model results were compared with field-observed data for matrix liquid, water potential, perched-water elevations, and gas-pressure measurements.

Characterizing moisture movement is the essential issue at Yucca Mountain. Here we briefly summarize the results from our flow modeling, while more discussions on flow model calibrations against measured moisture data are given in *Wu et al.* [2004b]. Field data for measured matrix-liquid saturation, water-potential data, and perched-water elevations are compared against 3-D model results using the three present-day infiltration maps. Matrix-liquid saturation, water-potential, and perched-water data used for these comparisons were taken from eleven boreholes (Table 2, Figures 1 and 3a). In general, the simulation results from the calibrated 3-D model are in good or reasonable agreement with the measured saturation and water-potential profiles, as well as with perched-water data from all measuring boreholes.

Comparison with Pneumatic Data: Calibration of the 3-D UZ model to pneumatic data or gas flow provides a practical method of estimating large-scale fracture permeability within the 3-D UZ system [*Ahlers et al.*, 1999]. The 3-D pneumatic simulation was run using a two-phase liquid and gas flow module of the TOUGH2 code [*Pruess*, 1991]. Note that because of the low percolation flux at the site, moisture data are found to be insensitive to fracture properties under ambient infiltration conditions and are insufficient for estimating fracture permeability. In addition, a UZ flow model capable of modeling gas flow is particularly important for studies of thermal loading, air circulation, and transport of gaseous-phase radionuclides after waste emplacement in the Yucca Mountain UZ.

Gas flow calibration is carried out under a steady-state water flow condition with the present-day-mean infiltration scenario and by matching field-measured pneumatic data from five boreholes of Table 2. In doing so, fracture permeability needs to be modified from values estimated by the 1-D inverse model for a number of 3-D model layers. In these calibrations, the gas flow model uses the UZ thermal model grid (Figure 3b), with similar boundary conditions as those in the flow model for infiltration and temperature prescribed on the ground surface and water table. Additional pneumatic boundary conditions are needed on the land-surface boundary for the gas phase, specifically as the time-dependent gas-pressure conditions, based on measured atmospheric barometric pressure data at the site. Since gas flow is a much more rapid process than liquid or heat flow in the UZ, water flow during pneumatic calibration is assumed to be at steady-state conditions, determined by steady-state flow simulation results under the present-day mean infiltration scenario.

To capture the details of periodic gas-pressure variations for ridge and valley values, the maximum time step is set to be 13,000 seconds in the 3-D model simulation. The results of these gas-flow simulations are then compared with field-measured pneumatic data from several boreholes simultaneously, to examine the results from the 1-D models [*Liu et al.*, 2003b]. The model calibration results indicated that modification of fractured rock properties, as estimated by 1-D inversion in the TSw layers, is necessary for matching field-observed gas pressures. In particular, it was found necessary to reduce the fracture permeability of the subunits within the TSw by a factor of 15, as well as for the PTn units by a factor from 1.8 to 21. In the top unit of the TCw, however, no adjustment in fracture permeability from the 1-D model inversions is made. This is because 1-D flow appears to provide a good approximation for gas flow through the top, shallow TCw unit. Figure 5 shows a comparison between the observed gas-pressure versus simulation results, in which the curve labeled "non-calibrated" is plotted using the simulations with the 1-D model estimated fracture properties and "calibrated" using the 3-D model results, with TSw subunit fracture permeability reduced by a factor of 15. As shown in Figure 5, 3-D model calibrated results significantly improve the model match of the observed gas-pressure data, whereas the simulations with non-calibrated or 1-D model fracture permeability overestimates gas pressure responses at the corresponding elevation.

Comparison of model simulation results and field-measured pneumatic data for borehole UZ-7a is shown in Figure 6. The lower fracture permeability needed for the 3-D model may be attributed to the original fracture permeability being estimated from inversion of 1-D models, allowing for 1-D vertical flow paths only. In a 3-D model, some high-gas-flux channels may exist, such as through faults or highly fractured zones, and 3-D gas flow is able to find and follow these high-permeability pathways with the least flow resistance. This also shows why 3-D model calibration is necessary for UZ model development.

Many comparisons between model-simulated pressures and field measurements have been made with and without fracture-permeability modifications, and the results show that the calibrated 3-D model has improved the match of the observation data from for all pneumatic data boreholes. Overall, a reduction by a factor of 15 for the TSw fracture permeability, as estimated from moisture and geochemical data, provides a better fit to observed pneumatic data for all locations and all time periods. The good match in Figure 6 indicates that after calibration, simulated gas pressures and their patterns of variations are consistent with observed values.

In addition to the model calibration efforts discussed in this section, many model verification studies have been carried out using moisture, pneumatic, temperature, field water injection and tracer-release testing, and geochemical data [*BSC*, 2004; *Wu et al.*, 2004]. These verification data have also been observed from boreholes and underground tunnels, but have not been used for model calibration with the base-case present-day infiltration flow scenario. In these verification cases, the UZ flow model results have been shown to be in agreement or consistent with the field data of moisture, temperature, pneumatics, and geochemical isotopes.

5. Flow Patterns and Analyses

The primary objective of modeling UZ flow at Yucca Mountain is to estimate percolation flux through the UZ system. This is because percolation is the most critical factor in assessing overall repository performance under current and future climates. However, *in situ* percolation fluxes of unsaturated flow at the site are in general too low to measure directly. Therefore, indirect data and model results are needed to estimate these flux values and their distributions. Even with the considerable progress made so far in characterizing the Yucca Mountain UZ through intensive geological, hydrological, and chemical studies, accurate estimates of percolation flux within the UZ remain a scientific challenge.

Past studies [e.g., *Wu et al.*, 2002a] have shown that it is very difficult even to quantify the range of percolation fluxes by using hydrological data alone. Percolation patterns inside the UZ strongly depend on infiltration rates and their spatial distribution, among other factors. Therefore, over the past two decades, significant research has been devoted to estimating infiltration rates using different methods and data sources [e.g., *Flint et al.,* 1996; *Hevesi and Flint,* 2000; *Flint et al.,* 2002; *Bodvarsson et al.*, 2003]. From these studies, the best estimates of present-day mean infiltration rates across the study area are in the range of several millimeters per year over the model domain. To further assess simulated UZ percolation fluxes for their relevance and reasonableness, this section presents percolation fluxes simulated by the calibrated 3-D UZ flow model and examines these percolation fluxes and their patterns using field-measured temperature and pore-water chloride data.

5.1 Simulated Percolation Fluxes

As listed in Table 3, a total of 18 3-D steady-state flow simulation scenarios are studied and used for analyzing percolation fluxes in this work. The 18 3-D flow simulations are decided by 9 (nine infiltration maps, See Table 1) multiplied by 2 (two sets of fracture-matrix parameters, one base case and one alternative, each sets having 3 different subsets of fracture and matrix properties). The classification of base-case and alternative parameters is based on model calibration results from the two different property sets for the PTn unit, because the base-case (or first-set) parameter models provide a better overall match to field data than the alternative properties [*BSC*, 2004; *Wu et al.,* 2004]. Note that the only difference between the base-case and alternative (or second-set) scenarios is the implementation of two different PTn parameter sets of fracture and properties or conceptual models of lateral flow. The objectives of investigating a large number of 3-D flow scenarios are (1) cover various uncertainties and possibilities related to the UZ flow patterns, and (2) investigate the effects of uncertainties with estimated infiltration rates and model parameters on simulated percolation fluxes, under current and future climates and different conceptual models.

Percolation Patterns at Repository: Percolation fluxes at the repository horizon, as predicted using the 18 3-D UZ flow simulation results of Table 3, are used for insight into percolation patterns. Figures 7 and 8 present two examples of percolation fluxes simulated at the repository level for the present-day climate (Figure 4) by the base-case and alternative models, respectively. A comparison of the calculated repository percolation fluxes (Figures 7 and 8) with the surface infiltration map (Figure 4) indicates that percolation fluxes at the proposed repository are different from surface infiltration patterns.

The major difference between percolation fluxes at the repository level (as shown in Figure 7) and surface infiltration patterns (Figure 4) are: (1) flow focusing into faults in the very northern part of the model domain (with the north coordinate > 237,000 m); (2) flow diverted into or near faults located in the middle and southern model domain; and (3) about several hundred m lateral flow of the high-infiltration zones to the east from north to south along the crest, as illustrated by the "lateral flow scale" on Figure 7. Note that flow redistribution or focusing in the very northern part of the model domain (beyond the repository block) results from the repository grid-layer horizon laterally intersecting the CHn zeolitic and perched-water zones, where major flow paths are through faults. On the other hand, the simulation results (Figure 8) with the alternative flow model shows a high flux distribution, a distribution very similar to that shown on infiltration maps (Figure 4) in the middle (except for the very northern part) of the model domain along the north-south mountain crest. Thus, judging from the alternative model results, smaller lateral flow occurs in the PTn in the area above the repository.

Further examination of all simulated fluxes at the repository level from different surface infiltration scenarios indicates that the lower the infiltration rates, the larger the lateral flow scales. This is because the lower infiltration results in "drier" conditions and stronger contrasts in capillary forces [*Wu et al.*, 2002b]. In comparison, the simulation results with the nine alternative flow fields show relatively small PTn lateral flow in the area above the repository.

Percolation fluxes within the repository footprint can be further analyzed using a frequency distribution that displays the average percentage of the repository area subject to a particular percolation rate. In this analysis, percolation rates are normalized with respect to the average infiltration rate for the climate scenario. For example, the flux rates are normalized by 4.4, 11.8, and 17.0 mm/yr (Table 1), respectively, for the three mean infiltration scenarios. The statistics of flux distributions is important to smaller-scale modeling studies of flow and transport and flow-focusing phenomena throughout the UZ. Furthermore, the frequency distribution of normalized percolation fluxes within the repository horizon from the 18 simulated flow-field analyses can be used to define a cumulative flux-frequency distribution, as shown in Figure 9, displaying a regression curve that incorporates the 18 flow fields. The cumulative frequency of Figure 9 can be used, for example, in selecting ambient flow-boundary conditions for smaller-scale modeling. The regression curve, with the equation given on the figure, may be used to correlate cumulative flux frequency within the repository with net infiltration rates for any future climatic scenarios. For example, using the equation with $x = 1$, 2, and 5 gives results of 60%, 88%, and 99%, respectively. This indicates that 60%, 88%, and 99% of the repository blocks are subject to less than normalized fluxes of 1, 2, and 5, respectively.

Percolation Patterns below Repository: Percolation fluxes below the repository horizon play a critical role in controlling the migration of radioactive waste from the repository to the water table. Figure 10 shows an example of the simulated percolation fluxes at the water table, using the base-case model flow simulation with the present-day, mean infiltration scenario. When compared to percolation fluxes at the repository for the different model results and infiltration scenarios, percolation fluxes at the water table reveal more flow focusing into faults while traveling through the CHn unit. This is caused by the impact of perched water and low-permeability zeolitic units on flow paths through these lower units. Similar flux distributions and patterns at the water table are also seen for both base-case and alternative model flow fields under different climates, as compared with Figure 10, which is primarily caused by strong effects of faults, zeolites, and perched-water zones in the CHn. These results show the PTn conceptual model makes insignificant impact on flow below the repository or through the CHn unit.

In addition to looking at flow simulation results for insight into flux patterns below the repository or at the water table, locations or areas where radionuclides are most likely to break through at the water table, or high-flux flow paths across the CHn, can also be identified using tracer-transport-simulation results. To assess tracer transport from the repository to the water table, we used two types of tracers, conservative (nonadsorbing) and reactive (adsorbing), in this study. An initial, constant-source concentration was specified for the fracture continuum gridblocks representing the repository, released at the starting time of simulation. In addition, hydrodynamic/mechanical dispersion through the fracture-matrix system is ignored, because sensitivity studies have indicated that mechanical dispersion has an insignificant effect [*Wu et al.,* 2002a]. A constant molecular diffusion coefficient of 3.2×10^{-11} m^2/s is used for the conservative component, and 1.6×10^{-10} m^2/s is selected for the reactive component (the two values are measurements for technetium and neptunium diffusion). For the conservative tracer, $K_d = 0$, and for the reactive tracer, $K_d = 4$ cc/g for zeolitic matrix, $K_d = 1$ cc/g for other matrix rock in TSw and CHn units, and $K_d = 0$ cc/g for all fractures and other units.

Tracer transport modeling was conducted with the T2R3D code [*Wu and Pruess, 2000*] using the same flow model grid (Figure 3a) and the dual-permeability approach for fracture-matrix interaction. In the transport simulation, the isothermal, unsaturated, steady-state flow fields of Table 3 were used as direct input to the T2R3D.

Figures 11 and 12 show cumulative and normalized mass-arrival contours at the water table at 1,000 years for the conservative and reactive tracers, respectively. The cumulative and normalized mass arrival is defined as cumulative mass that arrives at each grid column (or block) of the water table over time, normalized by the total initial mass released at the entire repository. The two figures present examples of breakthrough over the water table for conservative and reactive tracers under the present-day, mean infiltration rate (preq_mA). The two figures clearly indicate a significant difference between the two tracer-modeling results in distributions of tracer mass arrivals along the water table. Figure 11 shows that without adsorption, in 1,000 years, the conservative tracer has a much larger breakthrough area, covering the entire area directly below the repository footprint, spreading to the east in the north. At this time, about 40% of the total initial mass of conservative tracers has arrived at the water table. At the same time, only about 2% of the reactive tracer breaks through, and only along and near the major faults (Figure 12), owing to adsorption effects in the rock matrix. Similarly, breakthrough areas can be identified in different grid layers at different times, which indicate tracer transport paths or flow pathways below the repository.

5.2 Flow Pattern Analyses

Simulated percolation fluxes, as discussed above, are model results only. Their accuracy and relevance for representing actual UZ percolation needs further examination. This section presents a quantitative evaluation of such simulated percolation fluxes estimated from the large-scale 3-D UZ flow model. In particular, borehole temperature logs and pore-water chloride data are used to assess percolation patterns. This is because these two types of data are found to be more sensitive to deep percolation than other types of data collected from the site.

Examination Using Borehole Temperature Data: The site-scale UZ modeling investigations have relied on an ambient thermal model to simulate large-scale heat flow and geothermal conditions in the Yucca Mountain UZ [*Wu et al.*, 1999a]. In general, the thermal model represents ambient geothermal and moisture conditions, which in turn represents initial and boundary conditions for the mountain-scale thermal-hydrological, thermal-hydrological-chemical, and thermal-hydrological-mechanical coupled-process models [*BSC*, 2004]. A recent study [*Bodvarsson et al.*, 2003] shows that borehole temperature data are very useful in estimating percolation flux values in the UZ and provide an independent examination of the ranges for estimated surface net infiltration rates and simulated percolation fluxes.

In this study, heat flow simulations use a 3-D thermal model grid (Figure 3b), base-case UZ model parameters, and present-day mean infiltration rate to simulate advective and conductive steady-state heat-transfer processes within the UZ. The main objective here is to analyze the average present-day infiltration rate. To account for variation in average atmospheric temperature along the mountain surface, measured mean surface temperatures and a linear equation are used to correlate surface temperature with elevation, thus describing initial surface temperature conditions [*Wu et al.,* 1999a]. Temperature distributions at the bottom boundary of the thermal model are taken from deep-borehole-measured temperature profiles [*Sass et al.,* 1988] for an initial guess of the water-table-boundary temperature contours. Then, initially estimated ground surface and water table temperatures are further calibrated by comparing model results with field temperature measurements.

Under steady-state conditions, temperature profiles or geothermal gradients within the UZ are controlled by regional geothermal and weather conditions. In addition, these profiles and gradients are also related to formation thermal conductivity, net infiltration rates, and deep percolation fluxes. In thermal calculations, the surface net infiltration rate is fixed, based on the U. S. Geological Survey estimates (Table 1), and the temperatures from the initially specified values along the top boundary are slightly adjusted. These adjustments result in a better match with observed borehole data. The rationale behind the adjustment is, first, that insufficient temperature data were collected along the UZ model boundaries for accurate description of temperature distributions along the boundaries. Second, under steady-state moisture and heat-flow conditions, both top and bottom boundary temperatures vary spatially, but are constant with time, which leaves room for adjustments to fit steady-state temperature profiles measured from boreholes.

Figure 13 shows a model calibration result using measured temperature profiles in six boreholes (NRG-6, NRG-7a, SD-12, UZ#5, UZ-7a, and H-4) [*Sass et al.,* 1988; *Rousseau et al.*, 1998]. The figure shows a good match between measured and simulated temperatures for all six boreholes. Note that near the ground surface in the boreholes, observed temperatures show significant seasonal variations, which cannot be captured by the steady-state heat flow model. However, these seasonal changes in surface temperature have little impact on steady-state heat flow and field measured temperature profiles in the deeper (more than 20 m) UZ. Field data, as well as comparisons with steady-state simulation results in Figure 13, indicate that the ambient geothermal conditions can be approximated as steady state on the large-scale model.

Matching measured temperature profiles using simulation results along these boreholes at different locations, as shown in Figure 13, implies that percolation fluxes (as well as their spatial distributions estimated by the 3-D UZ model) are within a reasonable range of the actual percolation in the UZ. Otherwise, the study by *Bodvarsson et al.*[2003] indicates that if the surface infiltration rate is increased or decreased by a factor of 3 or more, temperature profiles can generally no longer be fitted by a 3-D model. This is because on average, a percolation flux of 5 mm/yr removes about 10 mW/m^2 of downward heat convection, which is about 25% of upward heat conduction, ~ 40 mW/m^2 [*Sass et al.*, 1988], through the UZ by ambient geothermal gradients. Any large increase or decrease (e.g., by a factor of 2 or more) of infiltration or percolation flux values in the model will lead to significant changes in downward heat convection or in geothermal gradients, such that model results will significantly deviate from observed temperature profiles.

Examination Using Geochemical Isotopic Data: The methodology for analyzing percolation flux using geochemical pore-water chloride (Cl) data is based on modeling studies of chloride transport processes in the UZ under different infiltration scenarios. Here we discuss the detailed rationale for using Cl to constrain the percolation fluxes. The results of Cl transport modeling is briefly described; more detailed discussion and results using chloride and other isotopic data are provided in *BSC* [2004] and *Wu et al.* [2004].

While field-measured moisture data are found to be relatively insensitive to percolation values, geochemical isotopic data provide valuable information by which to analyze the UZ system and help constrain the UZ percolation flux range [*Sonnenthal and Bodvarsson,* 1999]. For example, pore-water chemical concentration data can be used to calibrate the UZ model and to bound the infiltration fluxes [*Liu et al.,* 2003; *BSC,* 2004]. The distribution of isotopic chemical constituents such as chloride (Cl^-) in both liquid and solid phases [*Lu et al.*, 2003] of the UZ system depends on many factors, such as hydrological and geochemical processes, surface precipitation, evapotranspiration, fracture-matrix interactions of flow and transport, and the history of climate changes and recharge. Therefore, the current status of chemical components existing within the UZ, as measured from the site, will reveal some of the past and current percolation patterns, along with their spatial variations.

Measurements of chloride concentration data were made from pore waters extracted from field samples [*Fabryka-Martin et al.,* 2002; *Yang et al.*, 1996 and 1998] collected from a number of surface-based boreholes and two underground tunnels, the Exploratory Studies Facilities (ESF) and the Enhanced Characterization of Repository Block (ECRB) (Figures 1 and 3a). The source recharge of chloride on the ground surface to the transport model is estimated using precipitation, runon, and runoff [*Sonnenthal and Bodvarsson,* 1999], and is imposed on the top boundary under different infiltration scenarios.

All Cl transport simulations were run using the T2R3D code for 100,000 years to approximate the current, steady-state condition under the infiltration scenarios considered. Chloride is treated as a conservative component transported through the UZ, subject to advection, diffusion, and first-order decay. The mechanical dispersion effect through the fracture-matrix system was ignored. A constant molecular diffusion coefficient of 2.032×10^{-9} m^2/s is used for Cl matrix diffusion.

The three present-day infiltration rates for lower, mean, and upper bounds are used in chloride modeling. Each of the three infiltration maps corresponds to two 3-D flow fields (Table 3), i.e., the base-case (A) and alternative models (B) use the same surface infiltration maps. For example, the same present-day mean infiltration scenario leads to two flow fields: preq_mA of the base case and preq_mB of the alternative. This results in a total of six 3-D flow fields with three base cases and three alternatives, based on different parameter sets of different PTn conceptual models. Therefore, the difference predicted by the two flow-field results under the same infiltration scenario (e.g., preq_mA and preq_mB) is a function of input parameters or conceptual models. On the other hand, the difference in model predictions with the same conceptual models of base cases (i.e., preq_lA, preq_mA, preq_uA) or alternatives (preq_lB, preq_mB, preq_uB) with different infiltration scenarios results from the effects of infiltration rates. By comparing model results with field-observed chloride data using different parameter sets (or conceptual models) and infiltration rates, it may be possible to identify more suitable conceptual model,s as well as to estimate the range of net infiltration rates.

The modeled chloride concentrations and their field measurements are represented in Figure 14, as an example, along the underground tunnel of ECRB. Several comparisons with borehole data are presented in BSC [2004] and *Wu et al.* [2004]. As shown in Figure 14, modeled chloride distributions in the UZ are very sensitive to both conceptual models of the PTn and net surface infiltration rates. Comparisons of simulated and measured chloride concentrations in Figure 14 indicate that the simulations for mean infiltration of the base-case model (preq_mA) have overall better matches than the alternative model results (preq_mB). It is also shown that base-case model results (preq_uA) with upper-bound infiltration give reasonable matches compared to the mean infiltration results (preq_mA), while model results using lower-bound rates give the poorest fit. In general, high net infiltration results in lower chloride concentrations, whereas lower net infiltration gives high chloride concentrations within the UZ system.

The results, as shown in Figure 14, demonstrate that neither lower infiltration rates (preq_lA) nor alternative model results (preq_lB, preq_mB, and preq_uB) could match the measured Cl data well [*BSC,* 2004]. Comparisons between the model results for chloride distributions, using the six different flow modeling scenarios, can be useful in distinguishing which infiltration map or conceptual model is more appropriate for site characterization. In comparing simulated chloride distributions using the base-case model with the alternative models (e.g., Figure 14), we find that the base-case flow field simulation results under the present-day, mean infiltration rate consistently provide a better overall match with the observed chloride. As discussed before, the main difference between the base-case and alternative flow fields is whether there is large- or small-scale lateral flow within the PTn unit, with the base-case flow fields in general predicting relatively large lateral diversion. The model calibration results using chloride data show that large lateral diversion may exist in the PTn unit.

Even though the chloride data analyses discussed above indicate that there may be large-scale lateral flow within the PTn unit, the existence of whether such lateral flow diversion and the size of its spatial scale is currently debatable or uncertain. One study by *Flint et al.* [2003], using an analytical model, moisture data, and chloride-mass-balance calculations, implies insignificant lateral flow in the PTn. In particular, they correlate water potential data versus modeled net infiltration rates along the same cross section of the ECRB to show small lateral flow. However, another field seepage test shows that lateral flow through the PTn matrix is very strong *[Salve et al.*, 2003]. Nevertheless, this study demonstrates that pore-water chloride provides additional evidence for understanding PTn flow, which has a direct impact on chloride transport and distributions.

6. Concluding Remarks

This paper presents an integrated modeling approach as well as its application to a large-scale study characterizing percolation patterns in the unsaturated zone of Yucca Mountain, Nevada. In particular, a comprehensive modeling effort is made to quantify moisture movement or unsaturated flow patterns at the Yucca Mountain UZ using the integrated approach for taking account the multiple processes, including moisture flow, natural geochemical reaction and transport, and gas and heat flow, within the UZ system. The modeling results, based on the integrated modeling approach, provide a better understanding of percolation patterns and flow behavior within the Yucca Mountain UZ. More importantly, integration of different types of field-observed data, such as water potential, liquid saturation, perched water, gas pressure, chloride concentration, and temperature logs, into one single modeling analysis provides a rare opportunity to cross-examine and verify different process model results and various conceptualizations, which may be impossible to achieve when using only one or two types of data. This study demonstrates that integrated model calibrations and analyses make it possible to have consistent model predictions for different but interrelated hydrological, pneumatic, geochemical, and geothermal processes in the UZ.

Model results and analyses, supported by field-observed moisture, temperature and geochemical data, provide several insights into complex flow patterns through the UZ system. First, water may not straightly flow downward in a thick, heterogeneous unsaturated zone, and instead, it may be significantly diverted laterally towards the east along the sloping layers and focused into major faults, such as at the Yucca Mountain site. This lateral flow diversion in the upper unit is caused by a capillary-barrier effect in general. Second, all the flow simulation results indicate significant lateral flow diversion occurring at the CHn, resulting from the presence of perched water or thick low-permeability zeolitic layers. Under the current hydrogeological conceptualization, faults act as major flow paths through the CHn or below the repository horizon. In addition, the modeled percolation fluxes and their distributions show that fracture flow is dominant in the welded tuff, both at the potential repository horizon and at the water table, while matrix carries the majority of water percolation through the non-welded tuff.

This integrated study shows that the most important factors, which determine simulated percolation patterns in unsaturated fractured rock of Yucca Mmountain, include (1) a representative hydrogeological model for describing heterogeneity of fractured formation (layers, slopes, and faults), (2) fracture and matrix properties and their spatial distribution; and (3) surface net infiltration rate and its spatial distribution. In terms of applicability of data for validation of model predictions, borehole temperature data can be used to constrain the ranges of deep percolation rates. In comparison, geochemical isotopic data of chlroide, related to past climate history and current flow pathways, provides extremely useful information for percolation behavior within the UZ. In addition, it is found that for an unsaturated fracture-matrix system with highly permeable fractures and low-permeability matrx, subject to low net infiltration rate, fracture flow properties show relative insensitivity to water flow. In such cases, pneumatic data are among the best data source for estimating fracture permeability.

This study summarizes our current research effort to characterize UZ flow patterns at Yucca Mountain. As demonstrated in this work, the integrated methodology, integrating numerical models with various types of data and physical processes, provides a practical and promising approach for conducting large-scale site-characterization investigations in unsaturated fractured rock.

Acknowledgments

The authors would like to thank S. Mukhopadhyay and Dan Hawkes for their review of this paper. This work was supported by the Director, Office of Civilian Radioactive Waste Management, U.S. Department of Energy, through Memorandum Purchase Order EA9013MC5X between Bechtel SAIC Company, LLC, and the Ernest Orlando Lawrence Berkeley National Laboratory (Berkeley Lab). The support is provided to Berkeley Lab through the U.S. Department of Energy Contract No. DE-AC03-76SF00098

References

Ahlers, C. F., S. Finsterle, and G. S. Bodvarsson, Characterization and prediction of subsurface pneumatic response of at Yucca Mountain, Nevada, *Journal of Contaminant Hydrology*, 38 (1–3), 47–68, 1999.

Ahlers, C. F., T. M. Bandurraga, G. S. Bodvarsson, G. Chen, S. Finsterle, and Y. S. Wu. Summary of model calibration and sensitivity studies using the LBNL/USGS three-dimensional unsaturated zone site-scale model, Yucca Mountain Site Characterization Project Report, Lawrence Berkeley National Laboratory, Berkeley, CA, 1995a.

Ahlers, C. F., T. M., Bandurraga, G. S. Bodvarsson, G. Chen, S. Finsterle, and Y. S. Wu, Performance analysis of the LBNL/USGS three-dimensional unsaturated zone site-scale model, Yucca Mountain Project Milestone 3GLM105M, Lawrence Berkeley National Laboratory, Berkeley, CA, 1995b.

Bandurraga, T. M. and G. S. Bodvarsson, Calibrating hydrogeologic properties for the 3-D site-scale unsaturated zone model of Yucca Mountain, Nevada *Journal of Contaminant Hydrology*, 38 (1–3), 25-46, 1999.

Bodvarsson, G. S., E. Kwicklis, C Shan, and Y. S. Wu, Estimation of percolation flux from borehole temperature data at Yucca Mountain, Nevada, *Journal of Contaminant Hydrology*, 62-63, 3–22, 2003.

BSC (Bechtel SAIC Company), UZ flow models and submodels, Report MDL-NBS-HS-000006 REV002, Berkeley, CA, Lawrence Berkeley National Laboratory, Las Vegas, Nevada, CRWMS M&O, 2004.

BSC (Bechtel SAIC Company), *Analysis of Hydrologic Properties Data*, Research Report: MDL-NBS-HS-000014 REV 00, Lawrence Berkeley National laboratory, Las Vegas, Nevada, CRWMS M&O, 2003a.

BSC (Bechtel SAIC Company), *Calibrated Properties Model,* Report: MDL-NBS-HS-000003 REV 01, Lawrence Berkeley National laboratory, Las Vegas, Nevada, Bechtel SAIC Company, 2003b.

BSC (Bechtel SAIC Company), Simulation of net infiltration for modern and potential future climate, Report ANL-NBS-GS-000008. Denver, Colorado: U. S. Geological Survey, 2000a.

BSC (Bechtel SAIC Company), Future climate analysis, Report ANL-NBS-HS-000032. Denver, Colorado: U. S. Geological Survey, 2000b.

Buesch, D.C., R.W. Spengler, T. C. Moyer, and J.K. Geslin, Nomenclature and macroscopic identification of lithostratigraphic units of the Paintbrush group exposed at Yucca Mountain, Nevada, Report USGS OFR 94-469, U. S. Geological Survey, 1995.

Doughty, C, Investigation of conceptual and numerical approaches for evaluating moisture, gas, chemical, and heat transport in fractured unsaturated rock, *Journal of Contaminant Hydrology*, 38 (1–0-3), 69-106, 1999.

Fabryka-Martin, J., A. Meijer, B. Marshal, L. Neymark, J. Paces, J. Whelan, and A. Yang, Analysis of geochemical data for the unsaturated zone, Report ANL-NBS-HS-000017, Los Alamos, NM, Los Alamos National Laboratory, Las Vegas, Nevada, CRWMS M&O, 2002.

Flint, E. L., A. L. Flint, E. M. Kwicklis, J. T. Fabryka-Martin, and G. S. Bodvarsson, Estimating recharge at Yucca Mountain, Nevada, USA: comparison of methods, *Hydrogeology Journal*, 39, (10), 180-204, 2002.

Flint, A. L., L. E., Flint, and J. S. Selker, Influence of transitional volcanic strata on lateral diversion at Yucca Mountain, Nevada, *Water Resources Research*, 39, (4), 4-1–4-17, 2003.

Flint, A. L., J. A. Hevesi, and L. E. Flint, Conceptual and numerical model of infiltration for the Yucca Mountain area, Nevada, U.S. Geological Survey, Water-Resources Investigation Report-96, Denver, Colorado, 1996.

Liu, H. H., C. Doughty, and G. S. Bodvarsson, An active fracture model for unsaturated flow and transport in fractured rocks, *Water Resources Research*, 34, 2633–2646, 1998.

Liu, J., E. L. Sonnenthal, and G. S. Bodvarsson, Calibration of Yucca Mountain unsaturated zone using porewater chloride data, *Journal of Contaminant Hydrology,* 62-63, 231–236, 2003.

Lu, G., E. L. Sonnenthal and G.S. Bodvarsson, Implications of halide leaching on chlorine-36 studies at Yucca Mountain, Nevada. *Water Resour. Res.,* 10.1029/2003WR002546, 39(12), 1361-1375, 2003.

McLaren, R. G., P. A. Forsyth, E. A. Sudicky, J. E. VanderKwaak, F. W. Schwarltz, and J. H. Kessler, Flow and transport in fractured tuff at Yucca Mountain: numerical experiments on fast preferential flow mechanisms, *Journal of Contaminant Hydrology,* 43, 211–238, 2000.

Montazer, P. and W. E. Wilson, *Conceptual Hydrologic Model of Flow in the Unsaturated Zone, Yucca Mountain, Nevada.* Water-Resources Investigations Report 84-4345, Lakewood, Colorado: U.S. Geological Survey, 1984.

Moridis G. J., Q. Hu, Y. S. Wu, and G. S. Bodvarsson, Preliminary 3-D site-scale studies of radioactive colloid transport in the unsaturated zone at Yucca Mountain, Nevada, *Journal of Contaminant Hydrology*, 60, 251–286, 2003.

Pan, L., J. Hinds, C. Haukwa, C., Y. S. Wu, and G. S. Bodvarsson, *WinGrider: An Interactive Grid Generator for TOUGH2, Version 1.0* (Users' Manual), Earth Sciences Division, Lawrence Berkeley National Laboratory, Berkeley California, 2000.

Pollock, D. W., Simulation of fluid flow and energy transport processes associated with high-level radioactive waste disposal in unsaturated alluvium, *Water Resources Research*, 22 (5), 765–775, 1986.

Pruess, K., *TOUGH2-A General-Purpose Numerical Simulator for Multiphase Fluid and Heat Flow,* LBL-29400, Berkeley, California: Lawrence Berkeley Laboratory, 1991.

Pruess, K. and T. N. Narasimhan, A practical method for modeling fluid and heat flow in fractured porous media, *Soc. Pet. Eng. J.,* 25, 14-26, 1985.

Robinson, B. A., C. Li, and C. K. Ho, Performance assessment model development and analysis of radionuclide transport in the unsaturated zone, Yucca Mountain, Nevada, *Journal of Contaminant Hydrology,* 62-63, 249–268, 2003.

Robinson, B. A., A. V. Wolfsberg, H. S. Viswanathan, G. Bussod, C. G. Gable, and A. Meijer, The site-scale unsaturated zone transport model of Yucca Mountain, Las Alamos National Laboratories, Milestone SP25BMD, Las Alamos, New Mexico, 1997.

Robinson, B. A., A. V. Wolfsberg, H. S. Viswanathan, C. W. Gable, G. A. Zyvoloski, and H. J. Turin, Modeling of flow radionuclide migration and environmental isotope distributions at Yucca Mountain, Las Alamos National Laboratories, Milestone 3672, Las Alamos, New Mexico, 1996.

Rousseau J. P., E. M. Kwicklis, and C. Gillies (eds), Hydrogeology of the unsaturated zone, North Ramp area of the exploratory studies facility, Yucca Mountain, Nevada, U.S. Geological Survey, Water-Resources Investigations 98-4050, 1998.

Rulon, J., G. S. Bodvarsson, and P. Montazer, Preliminary numerical simulations of groundwater flow in the unsaturated zone, Yucca Mountain, Nevada, LBL-20553, Lawrence Berkeley National Laboratory, Berkeley, CA, 1986.

Salve, R., C. M. Oldenburg, J. S. Y. Wang, Fault-matrix interactions in nonwelded tuff of the paintbrush group at Yucca Mountain, *Journal of Contaminant Hydrology,* 62-63, 269-286, 2003.

Sass J. H., A. H. Lachenbruch, W. W. Dudley Jr., S. S. Priest, and R .J. Munroe, Temperature, thermal conductivity, and heat flow near Yucca Mountain, Nevada: some tectonic and hydrologic implications, USGS OFR-87-649, 1988.

Scott, R. B., and J. Bonk, Preliminary geologic map of Yucca Mountain, Nye County, Nevada, with geologic sections, Report USGS OFR-84-494, US Geological Survey, 1984.

Sonnenthal, E. L. and G. S. Bodvarsson, Constraints on the hydrology of the unsaturated zone of Yucca Mountain, NV from three-dimensional models of chloride and strontium geochmestry, *Journal of Contaminant Hydrology,* 38 (1-3), 107–106, 1999.

Tsang, Y. W. and K. Pruess, A study of thermally induced convection near a high-level nuclear waste repository in partially saturated fracture tuff, *Water Resources Research,* 23 (10), 1958–1966, 1987.

van Genuchten, M. Th., A closed-form equation for predicting the hydraulic conductivity of unsaturated soils, *Soil Sci. Soc. Amer. J.,* 44(5), 892–898, 1980.

Viswanathan, H. S., B. A. Robinson, A. J. Valocchi, A. J. and I. R. Triay, I. R. A Reactive transport model of neptunium migration from the potential repository at Yucca Mountain, *Journal of Hydrology*, 209, 251–280, 1998.

Wang, J. S. Y. and T. N. Narasimhan, Hydrologic modeling of vertical and lateral movement of partially saturated fluid flow near a fault zone at Yucca Mountain, SAND87-7070, Sandia National Laboratories and LBL-23510, Lawrence Berkeley National Laboratory, Berkeley, CA, 1987.

Warren, J. E. and P. J. Root, The behavior of naturally fractured reservoirs, *Soc. Pet. Eng. J.,* Trans., AIME, 228, 245-255, 1963.

Weeks, E. P., Effects of topography on gas flow in unsaturated fractured rock: Concepts and observations, flow and transport through unsaturated rock (D.D. Evens and T.J. Nicholson, eds.), geophysical Monograph 42, American Geophysical Union, Washington, D.C., 165–170, 1987.

Wittwer, C., G. Chen, G. S. Bodvarsson, M. Chornack, A. Flint, L. Flint, E. Kwicklis, and R. Spengler, Preliminary development of the LBL/USGS three-dimensional site-scale model of Yucca Mountain, Nevada, LBL-37356, Lawrence Berkeley National Laboratory, Berkeley, CA, 995.

Wittwer, C. S., G. S. Bodvarsson, M. P. Chornack, A. Flint, L.Flint, B. D. Lewis, R. W. Spengler, and C. A. Rautman, Design of a three-dimensional site-scale model for the unsaturated zone at Yucca Mountain, Nevada, *High Level Radioactive Waste Management, Proceedings of the Third International Conference, Las Vegas, Nevada, April 12-16, 1992,* 263–271, 1992.

Wu, Y. S., G. Lu, K. Zhang, and G. S. Bodvarsson, A mountain-scale model for characterizing unsaturated flow and transport in fractured tuffs of Yucca Mountain, *Vadose Zone Journal*, 3:796-805, 2004b.

Wu, Y. S., L. Pan, W. Zhang, and G. S. Bodvarsson, Characterization of flow and transport processes within the unsaturated zone of Yucca Mountain, Nevada, *Journal of Contaminant Hydrology,* 54, 215–247, 2002a.

Wu, Y. S., W. Zhang, L. Pan, J. Hinds, and G. S. Bodvarsson, Modeling capillary barriers in unsaturated fractured rock, *Water Resources Research*, 38 (11), 35-1–35-11, 2002b.

Wu, Y. S. and K. Pruess, Numerical simulation of non-isothermal multiphase tracer transport in heterogeneous fractured porous media, *Advances in Water Resources*, 23, 699–723, 2000.

Wu, Y. S., C. Haukwa, and G. S. Bodvarsson, A site-scale model for fluid and heat flow in the unsaturated zone of Yucca Mountain, Nevada, *Journal of Contaminant Hydrology,*. 38 (1-3), 185–217, 1999a.

Wu, Y. S., A. C. Ritcey, and G. A. S. Bodvarsson, A modeling study of perched water phenomena in the unsaturated zone at Yucca Mountain, *Journal of Contaminant Hydrology,* 38 (1-3), 157–184, 1999b.

Wu, Y.S., C.F. Ahlers, P. Fraser, A. Simmons and K. Pruess, *Software Qualification Of Selected TOUGH2 Modules*, Report LBL-39490; UC-800, Lawrence Berkeley National Laboratory, Berkeley, CA, 1996.

Yang, I. C., P. Yu, G. W. Rattray, and D. C. Thorstenson, Hydrochemical investigations and geochemical modeling in characterizing the unsaturated zone at Yucca Mountain, Nevada. U.S. Geological Survey Water Resources Investigation Report 98-4132, U.S. Geological Survey, Denver, Co., 1998.

Yang, I. C., G. W. Rattray, and P. Yu, Interpretation of chemical and isotopic data from boreholes in the unsaturated-zone at Yucca Mountain, Nevada. Water Resources Investigation Report 96-4058. U.S. Geological Survey, Denver, Co., 1996.

Table 1. Climate scenarios and infiltration rates (mm/year) averaged over the flow model domain

Climate Scenario	Lower-Bound Infiltration	Mean Infiltration	Upper-Bound Infiltration
Present-Day/Modern	1.3	4.4	10.7
Monsoon	4.4	11.8	19.2
Glacial Transition	2.4	17.0	31.7

Table 2. The field-measured data used in model calibration, including moisture data (matrix liquid saturation, matrix water potentials, and perched-water elevations), and pneumatic data, as observed from 14 boreholes and one underground tunnel of the Enhanced Characterization of Repository Block (ECRB)

Borehole or Tunnel	Liquid Saturation	Water Potential	Perched Water	Gas Pressure
G-2			X	
NRG#5				X
NRG-6		X		
NRG-7a	X		X	X
SD-6	X	X		
SD-7	X		X	X
SD-9	X		X	
SD-12	X	X	X	X
UZ-1				
UZ#4		X		
UZ-7a				X
UZ-14	X		X	
UZ#16	X			
WT-24	X	X	X	
ECRB		X		

Table 3. Nine base-case and nine alternative simulation scenarios associated with parameter sets and infiltration maps

Designation/Simulation*		**Infiltration Rate/Climate Scenario**
Base-Case[+]	**Alternative[+]**	
preq_lA	preq_lB	Present-day, lower-bound infiltration
preq_mA	preq_mB	Present-day, mean infiltration
preq_uA	preq_uB	Present-day, upper-bound infiltration
monq_lA	monq_lB	Monsoon, lower-bound infiltration
monq_mA	monq_mB	Monsoon, mean infiltration
monq_uA	monq_uB	Monsoon, upper- bound infiltration
glaq_lA	glaq_lB	Glacial transition, lower-bound infiltration
glaq_mA	glaq_mB	Glacial transition, mean infiltration
glaq_uA	glaq_uB	Glacial transition, upper-bound infiltration

[*] A denotes base-case and B alternative flow scenarios; l, m, and u stand for lower, mean, and upper bounds of infiltration rates for each climate scenarios, respectively.

[+] The base-case simulations are based on the base-case parameter sets; while the alternative simulations are done using the alternative parameter sets.

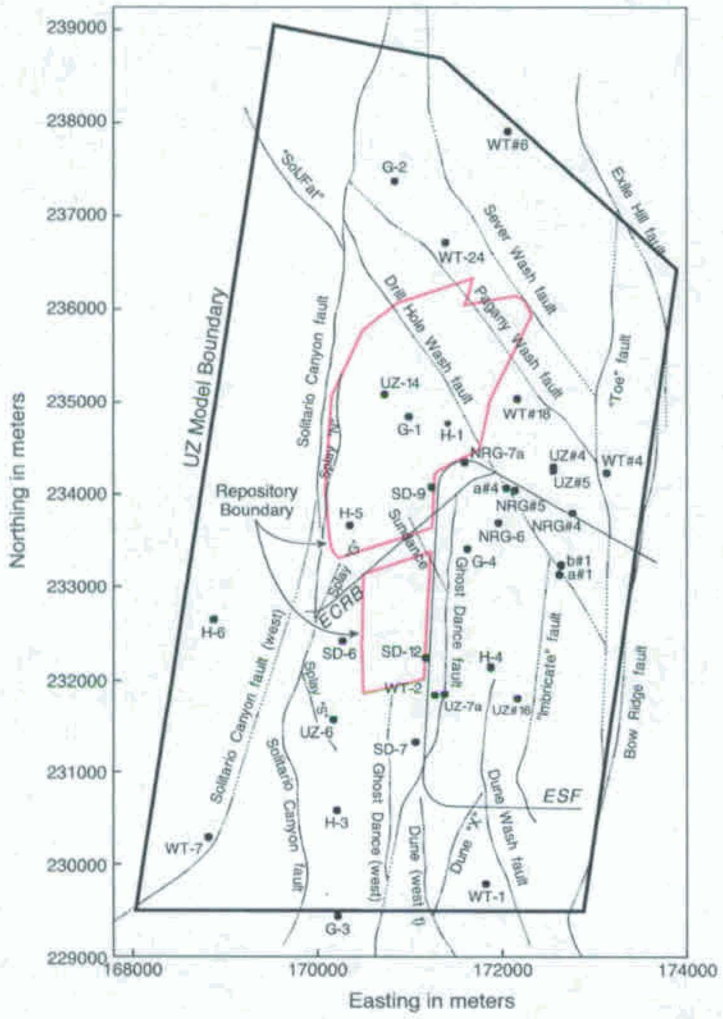

Figure 1. Plan view of the UZ model domain, showing the model boundary, the potential repository outline, major fault locations, the paths of the ESF and ECRB, and selected borehole locations

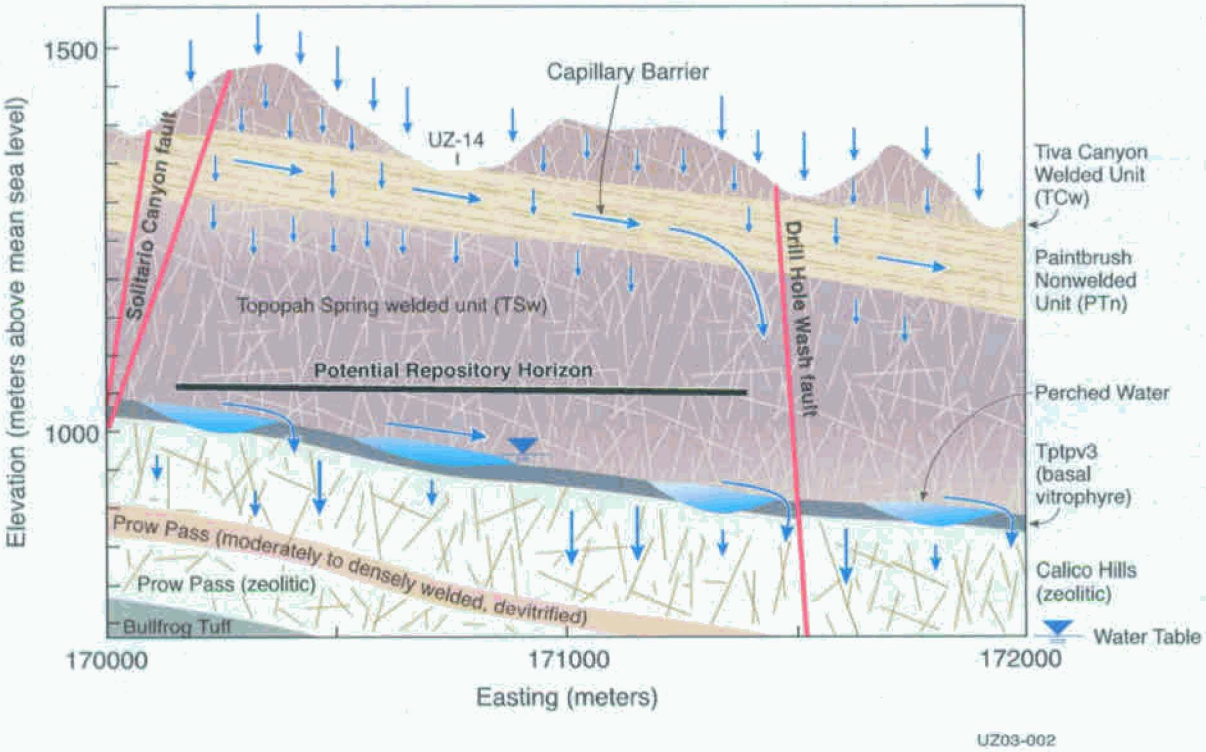

Figure 2. Schematic showing the conceptualized flow processes and effects of capillary barriers, major faults, and perched-water zones within a typical east-west cross section of the UZ flow model domain

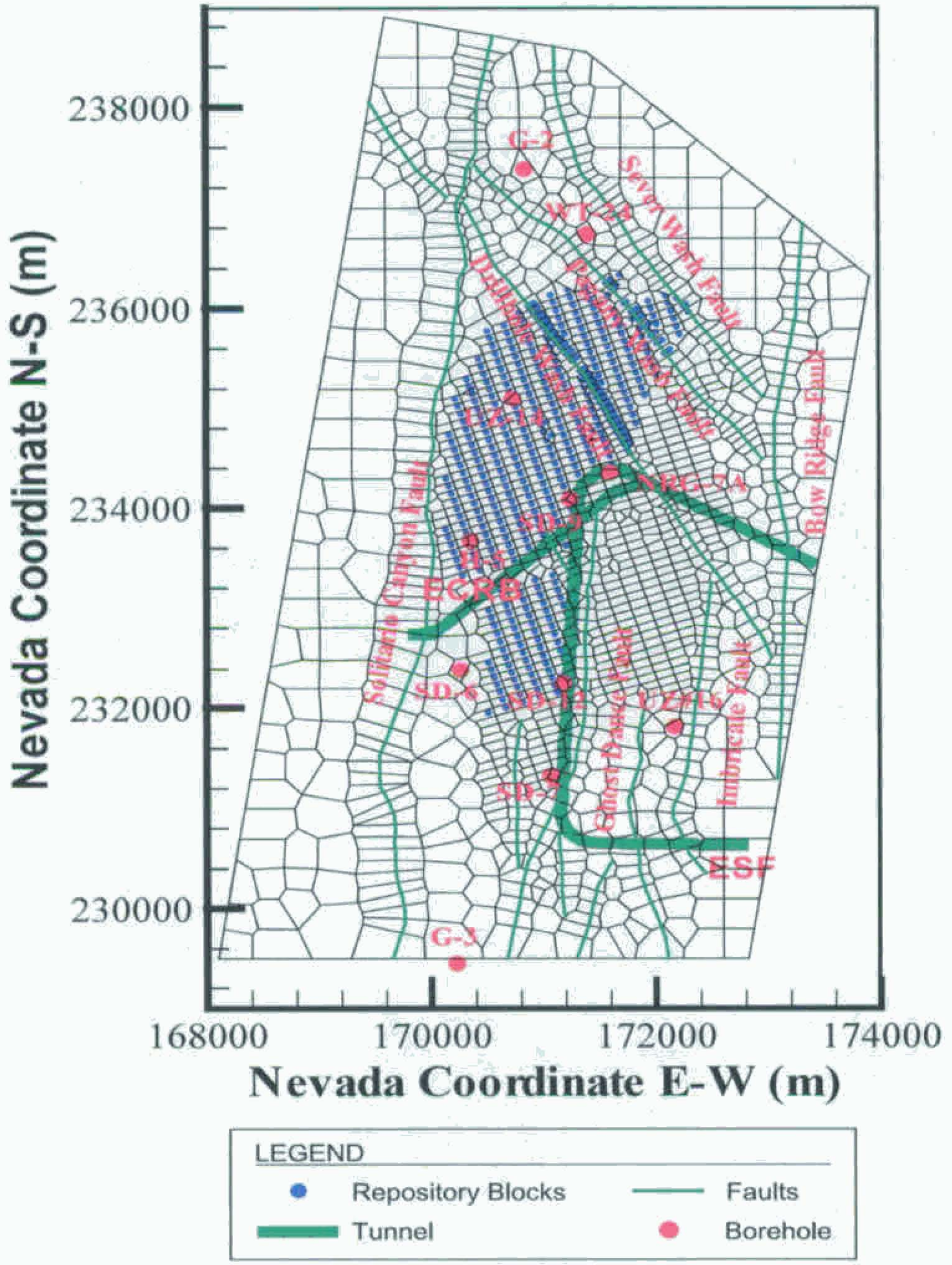

Figure 3a. Plan view of the 3-D UZ flow model grid, showing the model domain, faults incorporated, repository layout, and several borehole locations (modified from *BSC*, 2004)

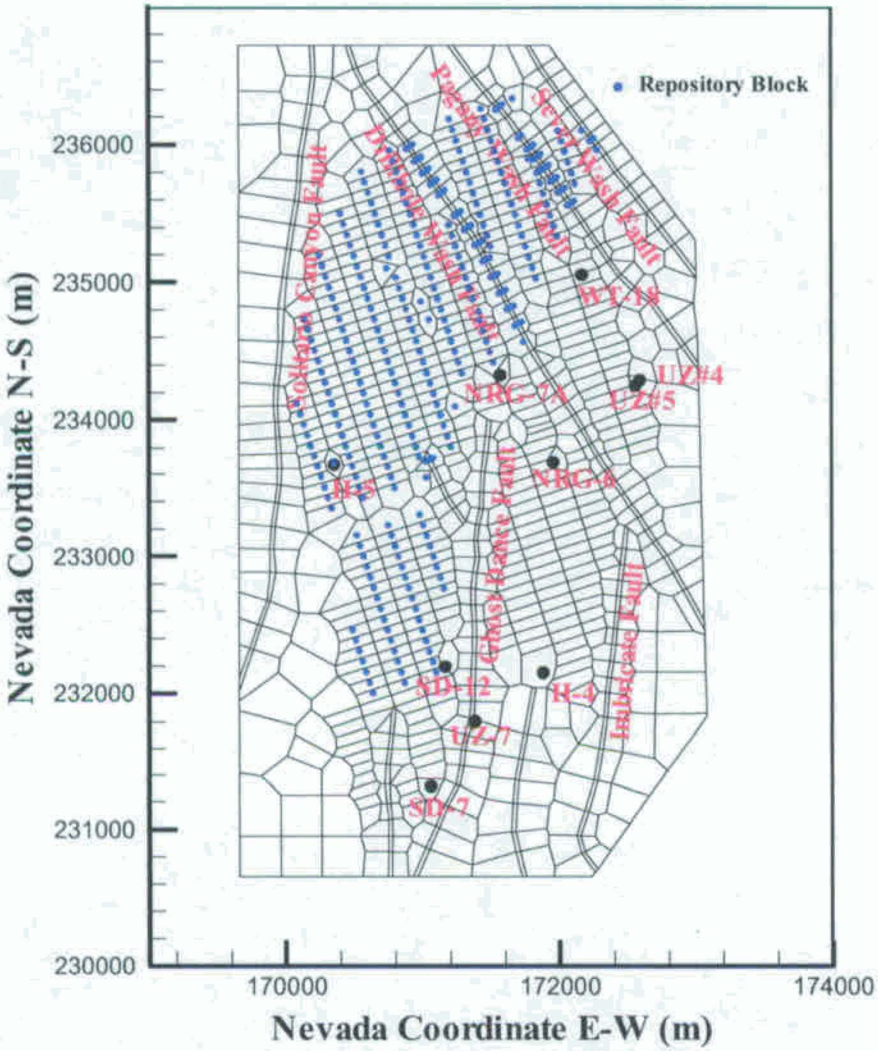

Figure 3b. Plan view of the 3-D thermal model grid showing a smaller model domain, used for modeling gas and heat flow

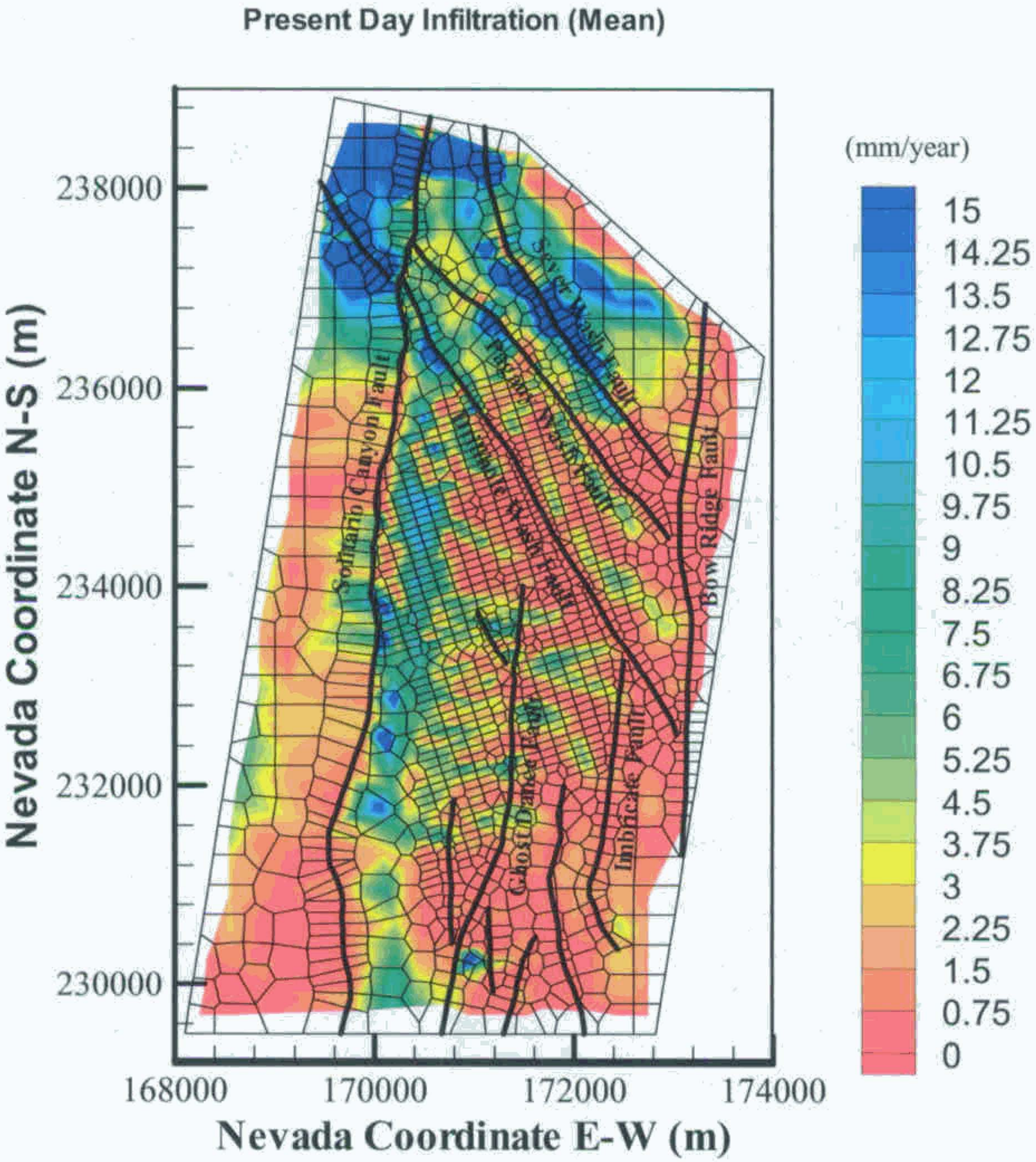

Figure 4. Plan view of net infiltration distributed over the 3-D UZ flow model grid for the present-day (base-case) mean infiltration scenario (modified from *Wu et al.*, 2004b)

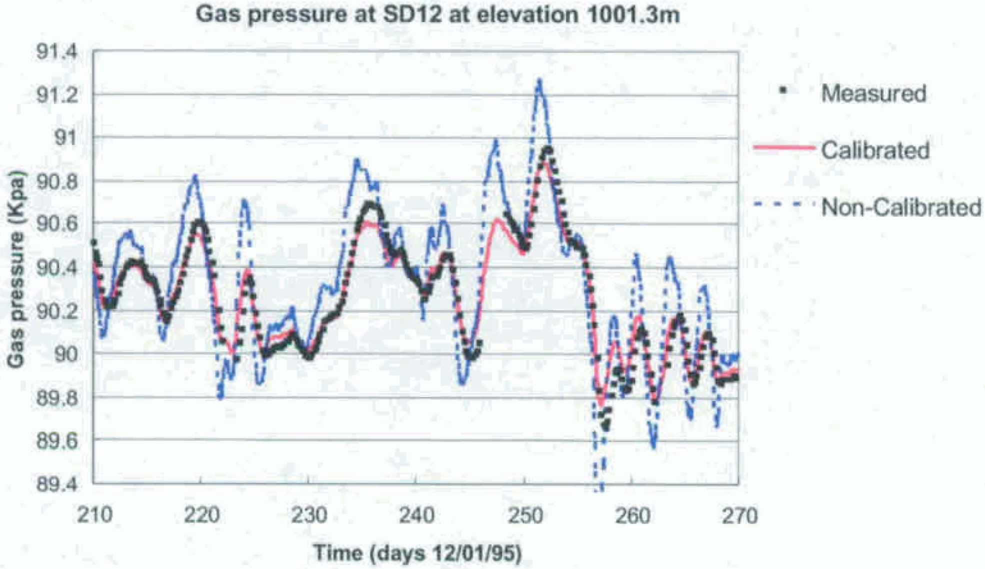

Figure 5. Comparison of simulated and observed gas pressures at borehole SD-12 during a 60-day period, using simulation results with and without 3-D calibration

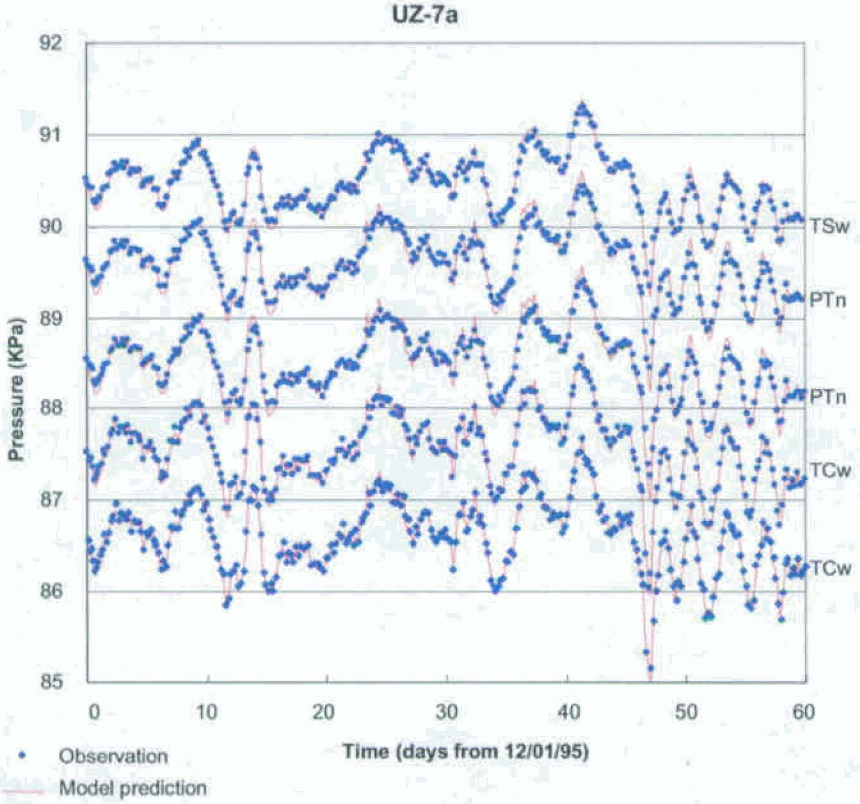

Figure 6. Comparison of simulated and observed gas pressure at borehole UZ-7a over a 60-day period

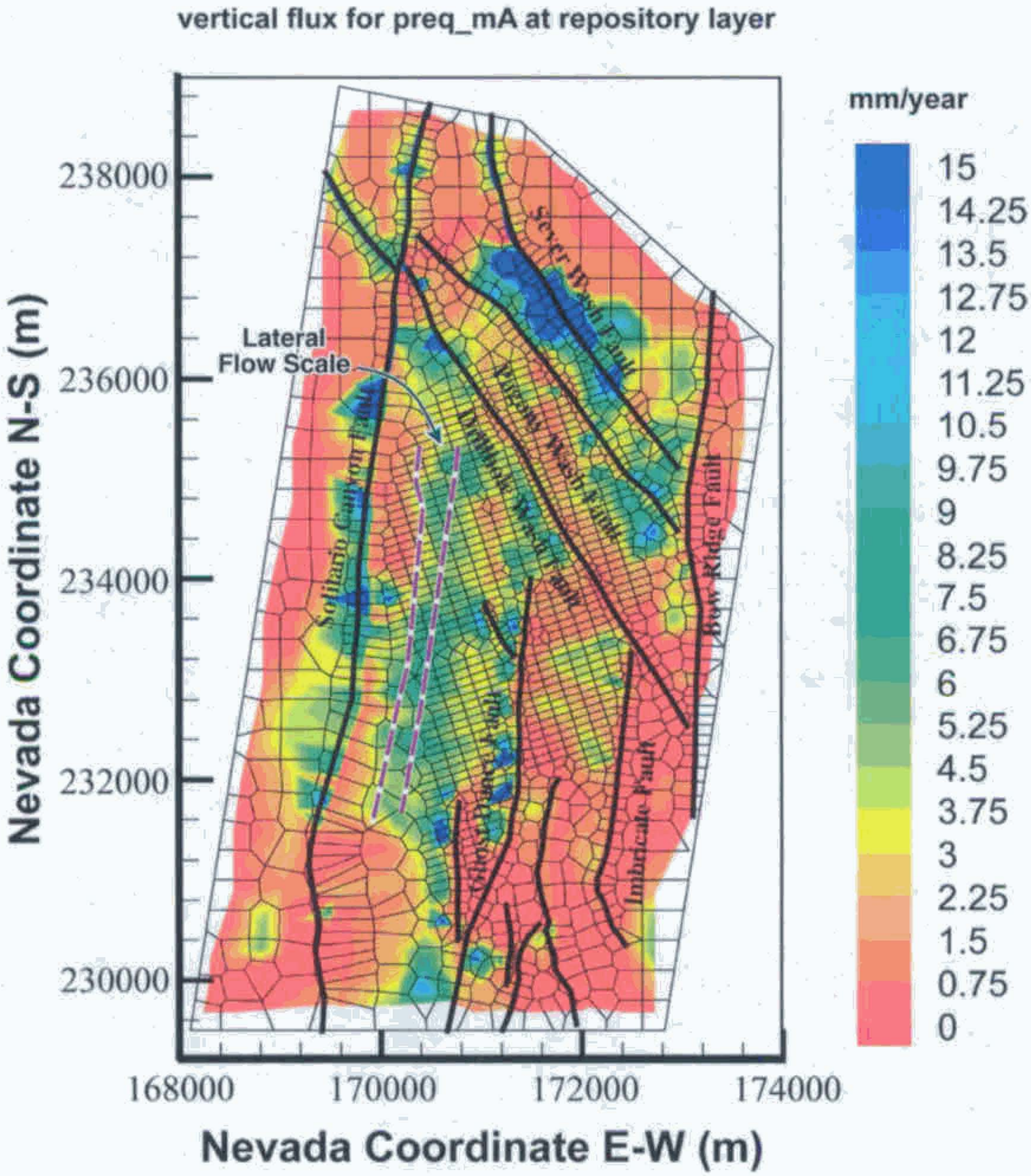

Figure 7. Simulated percolation fluxes at the repository horizon, using the present-day, mean infiltration scenario, base-case model results (preq_mA) (modified from *Wu et al.*, 2004b)

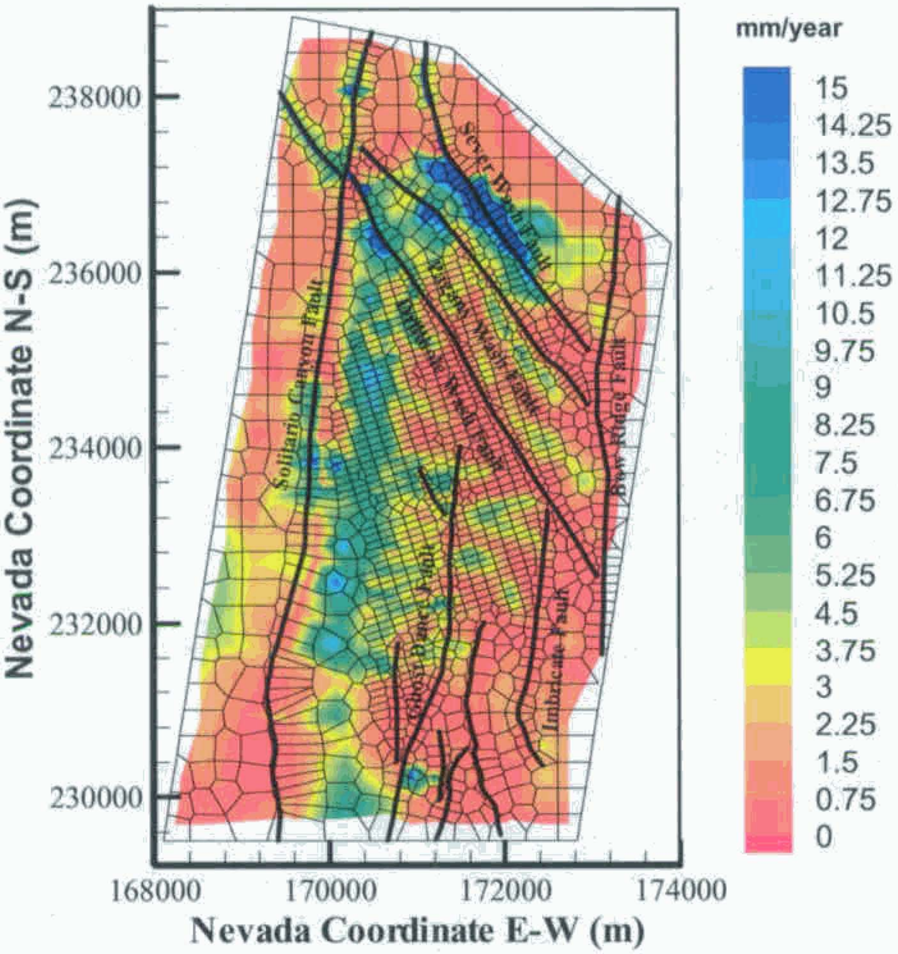

Figure 8. Simulated percolation fluxes at the repository horizon, using the present-day, mean infiltration scenario, alternative model results (preq_mB)

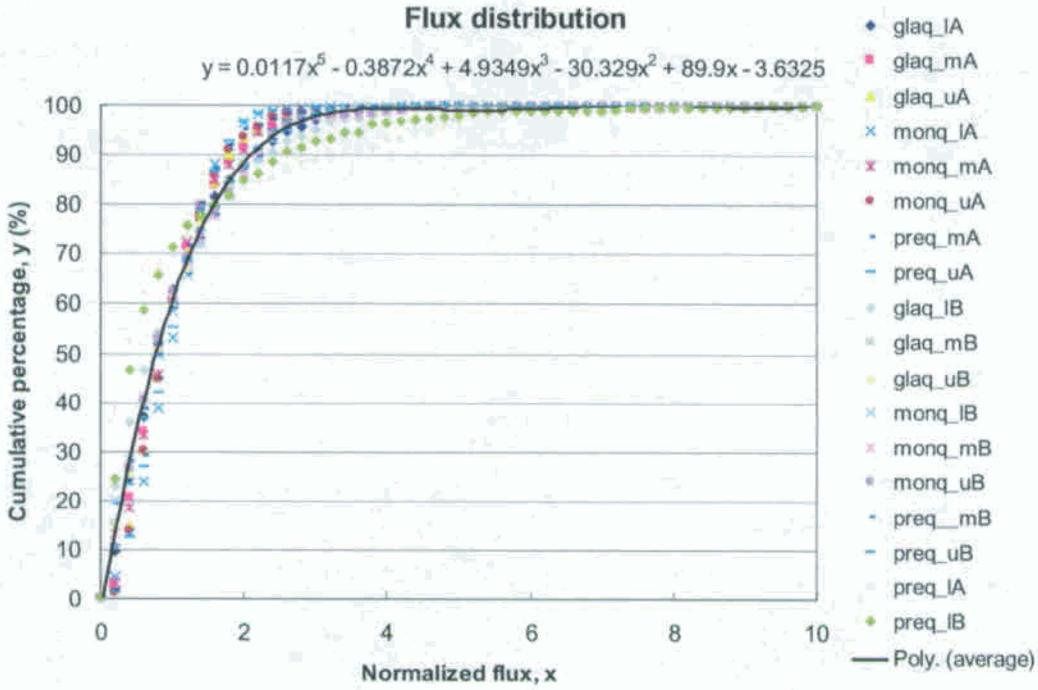

Figure 9. Cumulative flux distribution and range (as functions of normalized percolation flux within the repository) from the 18 flow fields (equation is valid for $0.05 < x < 10$, with x being normalized flux, and y bring cumulative area percentage)

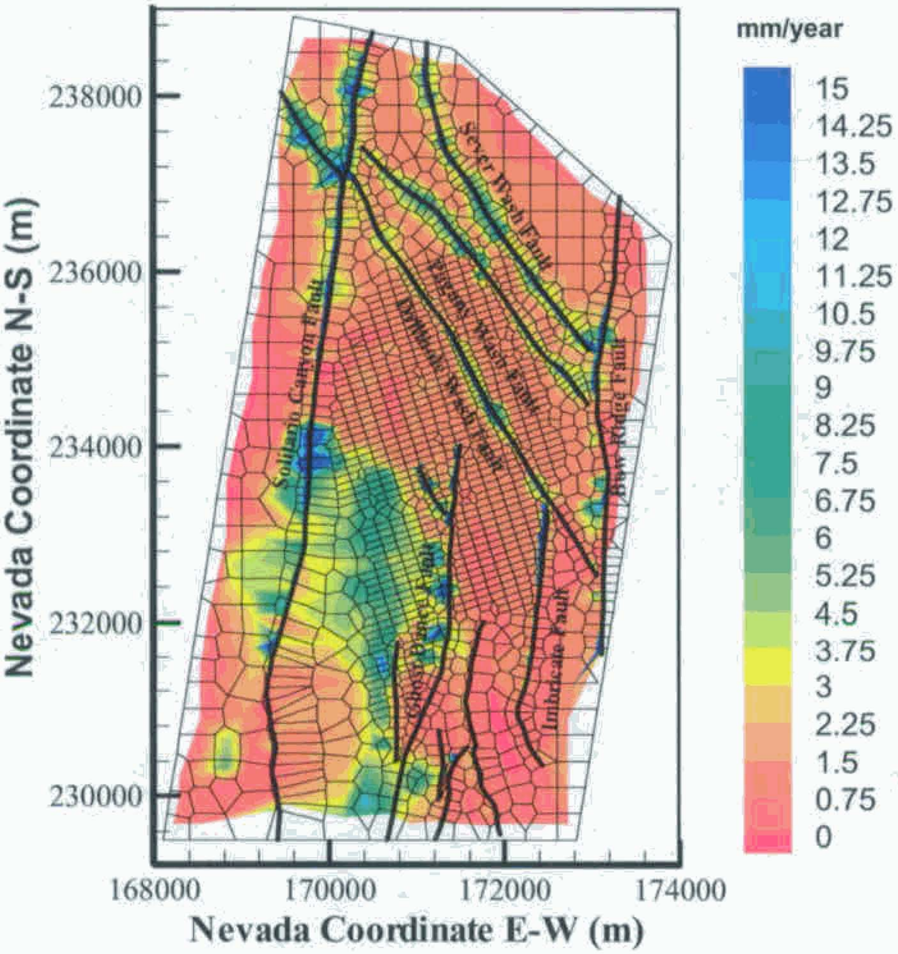

Figure 10. Simulated percolation fluxes at the water table, using the present-day, mean infiltration scenario, base-case model results (preq_mA)

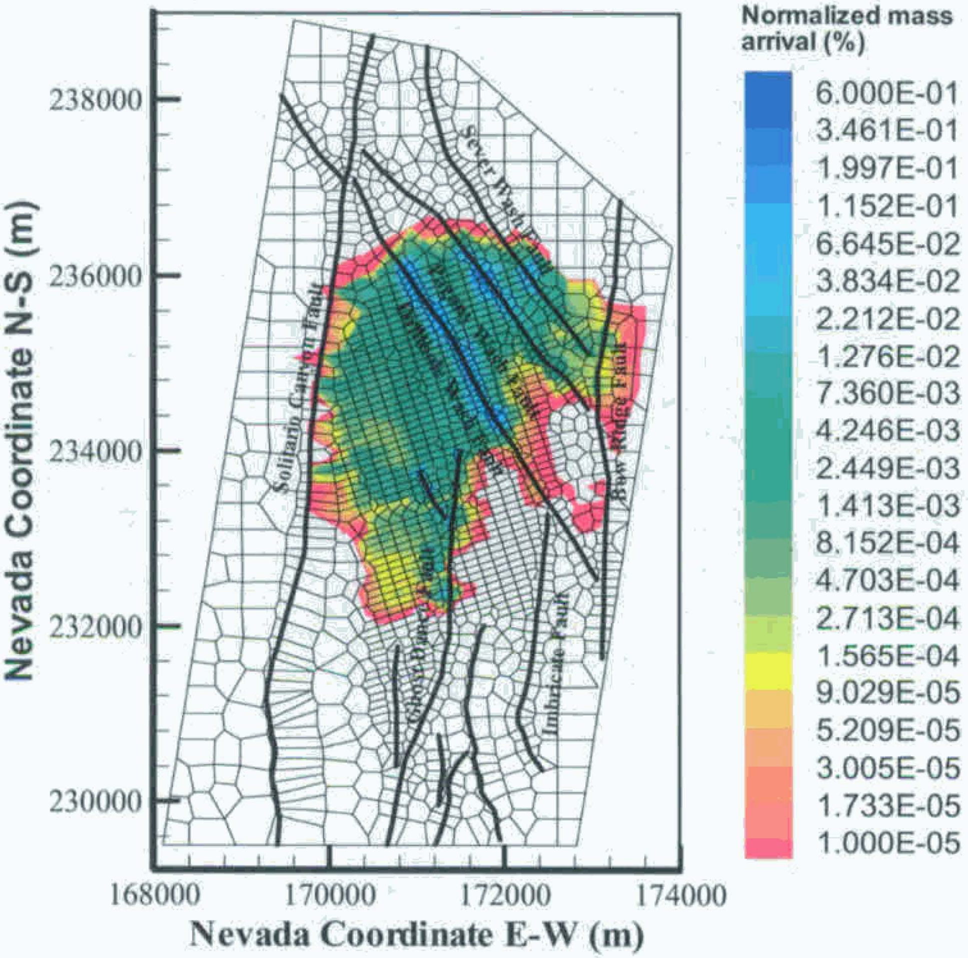

Figure 11. Simulated cumulative, normalized mass-arrival contours of a conservative tracer at the water table after 1,000 years, identifying potential breakthrough areas, using the present-day, mean infiltration scenario of the base-case model

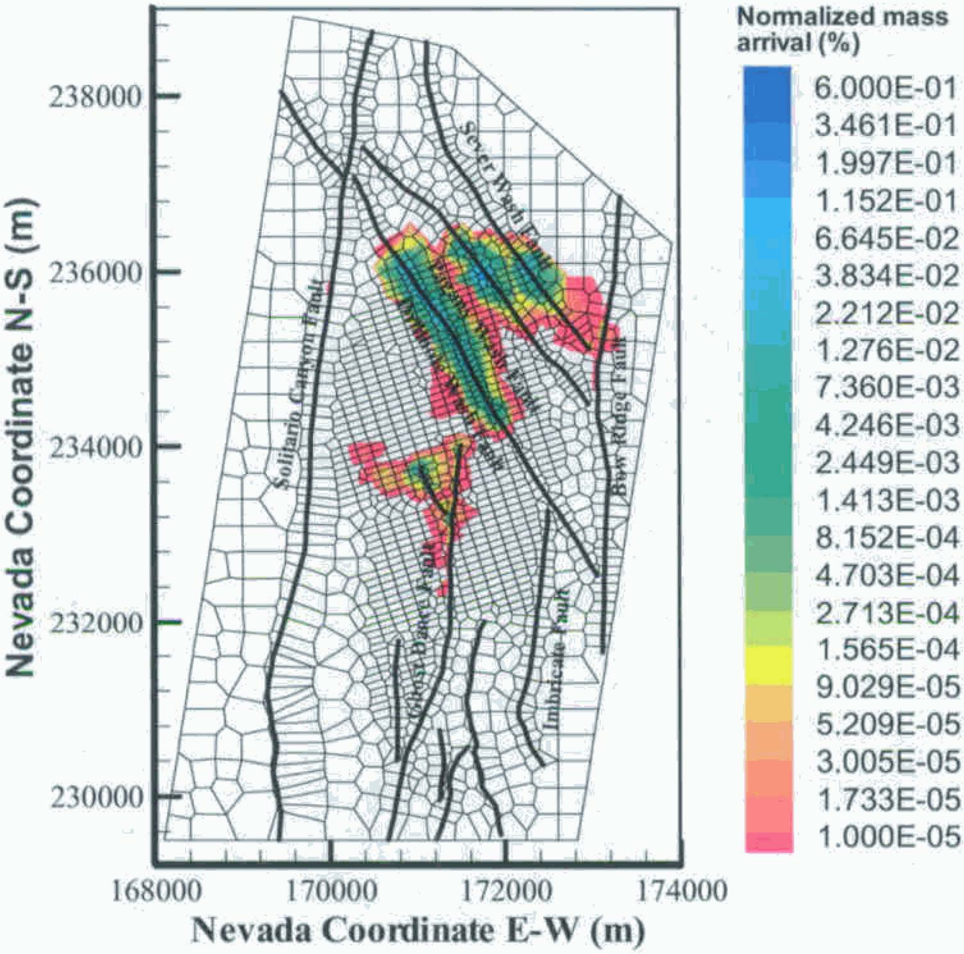

Figure 12. Simulated cumulative, normalized mass-arrival contours of a reactive tracer at the water table after 1,000 years, identifying potential breakthrough areas, using the present-day, mean infiltration scenario of the base-case model.

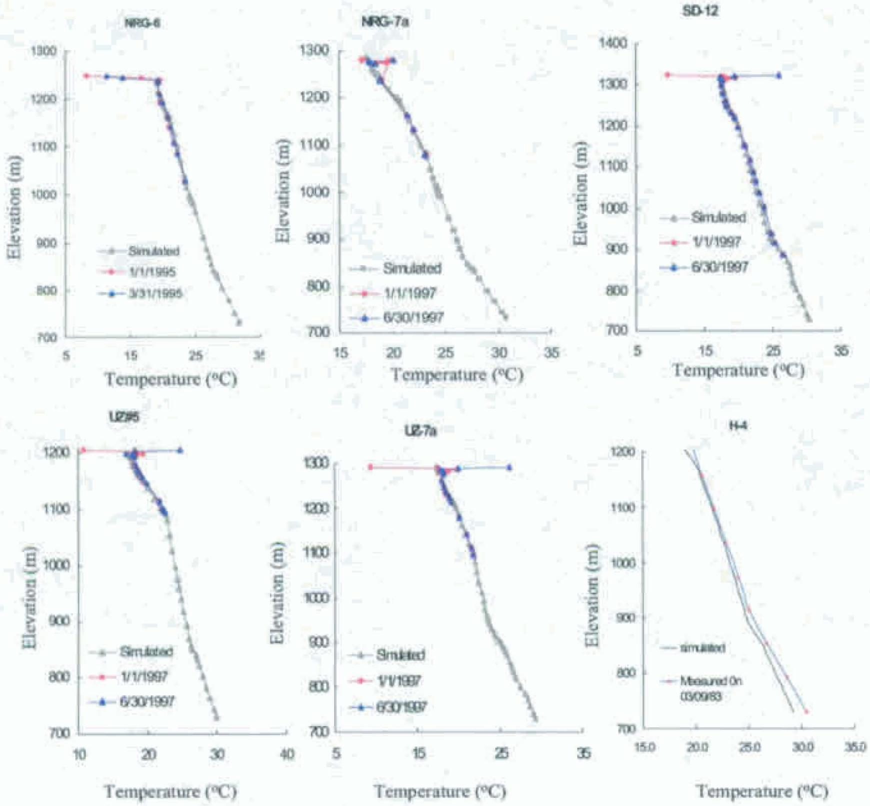

Figure 13. Comparisons between measured and simulated ambient temperature profiles for six boreholes under the present-day mean infiltration rate

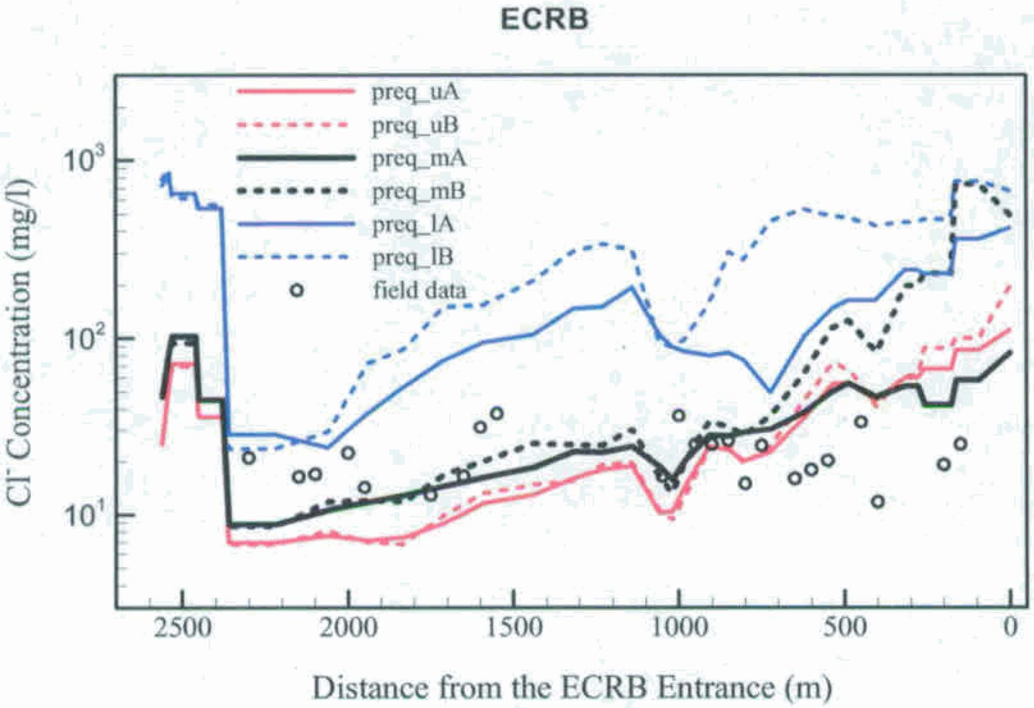

Figure 14. Comparison between measured and simulated chloride concentration (mg/L) profiles along the ECRB for present infiltration with mean, upper, and lower bound